Fatty acid isotopic fractionation in the diatom Chaetoceros muelleri

Marine Remize, Frédéric Planchon, Ai Ning Loh, Fabienne Le Grand, Margaux Mathieu-Resuge, Antoine Bideau, Rudolph Corvaisier, Aswani Volety, Philippe Soudant

Version of Record: https://www.sciencedirect.com/science/article/pii/S2211926420310328
Manuscript_3c14b599ceeb4ed4ffca13823de122da

Fatty acid isotopic fractionation in the diatom *Chaetoceros muelleri*

Marine REMIZE [1,2*], Frédéric PLANCHON [1], Ai Ning LOH [2], Fabienne LE GRAND [1], Margaux MATHIEU-RESUGE [1,3], Antoine BIDEAU [1], Rudolph CORVAISIER [1], Aswani VOLETY [4], Philippe SOUDANT [1*]

[1] Univ Brest, CNRS, IRD, Ifremer, UMR 6539 LEMAR F-29280 Plouzané, France

[2] University of North Carolina Wilmington, Department of Earth and Ocean Sciences, Center for Marine Science, 5600 Marvin K. Moss Ln, WILMINGTON NC 28403 USA

[3] WasserCluster Lunz – Inter-University Centre for Aquatic Ecosystem Research, Dr. Carl Kupelwieser Promenade 5 A-3293 Lunz am See, AUSTRIA

[4] Elon University, 50 Campus Drive, ELON NC 27244 USA

* Correspondence: marine.rem@hotmail.fr; philippe.soudant@univ-brest.fr

Abstract: Carbon isotopic fractionation was studied during the development of the diatom *Chaetoceros muelleri* grown in batch culture with ^{13}C-depleted CO_2 addition. Cellular and growth parameters and isotopic composition of dissolved inorganic carbon (DIC) and particulate organic carbon (POC) were monitored every two days, while the content and isotopic composition of individual fatty acid (FA) in polar lipid (PL) and neutral lipid (NL) were measured at 5th day (exponential phase) and 10th and 14th days (stationary phase). Continuous addition of petrochemical CO_2 to the algae led to a rapid and strong modification of DIC isotopic composition with cascading effects on particulate organic carbon and fatty acid isotopic compositions. Carbon isotope fractionation in *Chaetoceros muelleri* ranged from 17‰ to 25‰ and changed according to culture phases. Isotopic fractionation into FA was overall similar between PL and NL and was systematically higher than in POC. During the exponential growth phase, the isotopic composition of individual FAs varied from -51.3‰ to -58.4‰. During this phase, large differences in the isotopic compositions between FA were observed. Polyunsaturated FA (PUFA) such as 16:3n-4, 18:4n-3, and 20:5n-3 were more strongly ^{13}C-depleted than other FA such as 14:0, 16:0, 16:1n-7 or 18:1n-9. These results show how isotopic effects occur during the desaturation and elongation phase (for 20:5n-3 leading to their synthesis). Such isotopic effects were also supported by the lower $\delta^{13}C$ of averaged $\delta^{13}C$ of Saturated FA (SFA) and Monounsaturated FA (MUFA) as compared to those of PUFA. However, during the stationary phase, FA isotopic compositions were less variable according to POC while SFA and MUFA were more depleted than PUFA. Our study underlined the importance of consideration of phytoplankton growth phase when conducting ecological and biogeochemical studies as they appeared to strongly control phytoplankton carbon isotopic composition.

Keywords: Fractionation, stable isotopes, photosynthesis, phytoplankton, *Chaetoceros muelleri*, fatty acid synthesis.

1. INTRODUCTION

Global oceans and marine ecosystems are currently under significant threats due to increasing levels of atmospheric CO_2 and on-going climate change. At the base of marine ecosystems, phytoplankton groups are diverse and widely distributed and are likely to be impacted by these climatic changes. Indeed, in response to changes in environmental factors, photosynthetic organisms can modify their physiology and can modulate their productivity. For example, their lipid membrane composition changes with temperature [1-3]. Among phytoplankton taxa of importance at a global scale, diatoms are ubiquitous, found from cold to warm waters, and they account for about half of the global primary production [4]. Any alteration to their distribution, diversity, and production in response to global changes are expected to have tremendous effects on marine ecosystems.

The stable isotopic composition of carbon (ratio of ^{13}C vs ^{12}C expressed as $\delta^{13}C$ against the VPDB reference standard) is widely used for studying the on-going changes and their impacts on ecosystem-related processes in the different oceanic carbon pools (inorganic, organic, dissolved, particulate, sedimentary), and has proven to be a useful tracer. For example, the $\delta^{13}C$ of Dissolved Inorganic Carbon ($\delta^{13}C$-DIC) and its recent decrease due to the introduction of CO_2 from fossil fuels with light isotopic composition (the so-called Suess Effect) have been used to infer quantitative estimates of oceanic uptake of anthropogenic CO_2 (e.g. Gruber and Keeling [5]). This descriptive capability of $\delta^{13}C$ concerns also the organic carbon pool, which is derived primarily from marine photosynthetic activity. The $\delta^{13}C$ of bulk particulate organic carbon ($\delta^{13}C$-POC), and by extension of any organic compounds synthesized by marine algae (pigments, sugar, proteins, and lipids) provide substantial information on ecosystem dynamics as well as environmental and biogeochemical parameters. However, deciphering this information has proven to be particularly challenging since biological fractionation of carbon isotopes is governed by multiple factors.

During photosynthesis, phytoplankton incorporates aqueous CO_2, assumed to be available in excess in the marine environment [6] and converts it into organic carbon. This process preferentially uses the light isotope (^{12}C) over the heavy one (^{13}C), leading to a progressive depletion of ^{12}C relative to ^{13}C in the residual aqueous pool. Carbon fixation by ribulose-1,5-biphosphate carboxylase/oxygenase (RUBISCO) and β-carboxylases during photosynthesis, is responsible for the strongest isotopic effect [6-8] and varies according to RUBISCO types [9, 10]. Commonly, RUBISCO fractionation value is assumed to be around 25‰ [11, 12], but this value

has been revisited recently. Fractionation factor by type IA or IB RUBISCO appears to be close to the consensus value of 25‰, while fractionation by type II RUBISCO, occurring in some diatoms, is lower, around 18-20‰ [10].

The factors influencing carbon isotope fractionation in planktonic communities have been investigated through various i*n situ* studies [13, 14] as well as from culture experiments performed in batch [15-18] or chemostat [12, 19] and with variable CO_2 levels. Isotopic composition of phytoplankton depends on several factors including the species considered [20-22], the physiological status, the growth rate and the cell size [23]. It is also dependent on the species of inorganic carbon that is assimilated by the alga. In case of limited availability of CO_2, HCO_3^- via carbon concentrating mechanisms (CCM) can be used alternatively as a substrate for enzymatic fixation and can change the isotopic composition of organic carbon [7, 24].

Particulate organic carbon of phytoplankton is composed of different types of organic compounds whose signatures can be substantially different. Carbon isotopes are not distributed uniformly among lipids, carbohydrates, and proteins [14, 25, 26]. The lipid fraction is more depleted in ^{13}C relative to bulk POC or other main compounds [27, 28]. As for bulk carbon, the isotopic composition of lipids varies according to several factors: the isotopic composition of the carbon source [27, 29], the biosynthetic routes used to produce lipids [28, 30], the lipid classes [30], the compartmentalization of the organelles within the cell [29] and the physiology of phytoplankton [29]. Studying fractionation into lipids can then give further information on the fate of carbon after its enzymatic fixation by RUBISCO.

However, carbon fractionation remains not fully understood and rarely combined with physiological and cellular parameters. Utilizing culture experiments, this study focuses on the understanding of the processes responsible for carbon isotope fractionation during the development of the diatom *Chaetoceros muelleri*. Diatoms are responsible of around 40% of the global primary production [4] and characterized by a high 20:5n-3 content. The alga was grown with a constant supply of CO_2 of petrochemical origin (i.e., depleted in ^{13}C), which has been rarely applied to culture experiments and monitored for 24 days. Using compounds-specific stable isotope analysis (CSIA), our goal is to resolve the carbon isotope fractionation in fatty acids (FA) in comparison with the bulk carbon fractionation during the growth of *C. muelleri*. FA profiles and isotopic signatures have been followed during three-time points during the diatom culture and corresponding to different growth stages (exponential and stationary phases).

2. MATERIAL & METHODS

2.1. Culture conditions and experimental strains

Monospecific cultures were conducted with the marine diatom *Chaetoceros muelleri* (strain CCAP 1010-3 obtained from the CCAP culture collection, formerly listed as *Chaetoceros neogracile* VanLandingham 1968). The inoculum was initially transferred in a filtered sterile natural seawater and implemented with nutrients (Walne's medium) (Andersen, 2005). Cells were grown in batch (2 L balloon) at 19°C under continuous light and CO_2 addition for 24 days. The CO_2 gas added to the culture was of petrochemical origin and was strongly depleted in ^{13}C ($\delta^{13}C$-CO_2 = -37.7 ‰). The experimental set up was designed to produce a sufficient quantity of biomass, allowing detailed monitoring in triplicates of carbon isotopic composition of both POC and FA during algal growth.

2.2. Sample collection

Sampling for flow cytometry analysis (2 mL) was performed every two days for 24 days for a total of 16 samples. For Particulate Organic Carbon (POC) and Dissolved Inorganic Carbon (DIC) concentrations and stable isotopic compositions, samples were collected every four days (t_0, t_5, t_{10}, t_{14}, t_{19} and t_{24}). A volume between 15 mL to 50 mL according to cell concentration and filter saturation was filtered through pre-combusted 0.7 µm nominal pore-size glass fiber filters (Whatman GF/F), then dried at 55°C and stored at room temperature until analysis. DIC samples were collected from the filtrate of POC samples. Twelve mL was poured in Labco Exetainer tubes, poisoned with 20 µL of $HgCl_2$, and stored at 4°C until analysis. For FA concentration and isotopic composition, samples were collected at t_0, t_5, t_{10} and t_{14}. Samples at t_0 were sampled from the inoculum directly before transplanting in culture balloons. Twenty mL of culture was filtered on a pre-combusted 47 mm GF/F filter (porosity 0.7 µm), and boiling water was directly added after filtration to stop lipases activity. To extract lipids, the filter was immersed into 6 mL of 2:1 (v:v) chloroform:methanol solvent mixture. All extracts were flushed with nitrogen and stored at -20 °C until analysis.

2.3. Flow cytometry analysis

Cellular variables were measured using a FACScalibur (BD Biosciences, San Jose, CA, USA) flow cytometer with a 488 nm blue laser, detectors of forward (FSC) and side (SSC) light scatter, and three fluorescence detectors: green (525/30 nm), yellow (583/26 nm) and red (680/30 nm). Forward scatter (forward

scatter, FSC), side scatter (side scatter, SSC), and red fluorescence (FL3, red emission filter long pass, 670 nm) were used to select the algae population. FSC and SSC informs the relative size and complexity of cells, while red fluorescence is related to cell chlorophyll content.

Two fluorescent probes were used to evaluate viability and lipid content, according to Lelong, et al. [31] and Seoane, et al. [32]. The SYTOX Green (Molecular Probes, Invitrogen, Eugene, OR, USA, a final concentration of 0.05 µM) binds to the DNA of a permeable or permeabilized cell and was used to estimate the percentage of dead cells in culture sample [31]. The BODIPY probe (BODIPY 505/515 FL; Thermo-Fisher Scientific, Waltham, MA, USA, a final concentration of 10 mM) was used as a proxy of lipid reserves as it stains lipid droplets within microalgae cells [32]. Cytometric measurements were performed on live samples right after sampling with or without fluorescent probes every two days.

The concentration of bacteria was also monitored during the experiment, according to Seoane, et al. [32], using SYBR®Green (Molecular Probes #S7563, Invitrogen, Eugene, OR, USA). This DNA staining fluorescence probe allows the detection of DNA stained bacteria on FL1 detector (Green fluorescence). Results are expressed as the concentration of bacteria cells per mL.

2.4. POC concentration and stable isotope analysis

The filter for POC concentration and isotopic composition was first fumed with hydrochloric acid to remove particulate inorganic carbon, subsampled with a 13 mm punch, and encapsulated for POC concentration and isotopic composition. Analyses were performed using an elemental analyzer (EA, Flash 2000; Thermo Scientific, Waltham, MA, USA) coupled to a Delta V+ isotope ratio mass spectrometer (Thermo Scientific, Waltham, MA, USA) at the Pôle Spectrométrie Océan (PSO, Brest, France). For POC concentrations, acetanilide standards were used for the calibration, and results are reported in µmol.kg^{-1}. Carbon isotope ratios are expressed in delta notation (δ^{13}C-POC) in per mil (‰) as follow:

$$\delta^{13}C_{sample} = \left(\frac{\left(\frac{13C}{12C}\right)_{sample}}{\left(\frac{13C}{12C}\right)_{std}} - 1 \right) \times 1000 \qquad (1)$$

where $(^{13}C/^{12}C)_{std}$ is the ratio of the reference standard Vienna-Pee Dee Belemnite (V-PDB). For δ^{13}C-POC, raw results obtained from the spectrometer were corrected for mass drift, the blank contribution from the filter. They were scaled to V-PDB using the certified reference material and in-house standards listed in **Table 1**. The overall precision of the method estimated from routine replicates of *in-house* standards was 0.3‰.

2.5. DIC concentration and stable isotope analysis

For the DIC concentration and isotopic composition, the sample preparation was made according to Assayag, et al. [33] as follow: 1 mL subsample was added to a mixing tube and flushed with ultra-pure helium to avoid contamination from residual air, then 23 droplets of phosphoric acid were introduced to convert all DIC species into CO_2 [33]. After 15 hours equilibration time at room temperature, CO_2 and $\delta^{13}C$-CO_2 were measured in the headspace by Gas Bench coupled to a Delta Plus mass spectrometer from Thermo Scientific, Waltham, MA, USA (GB-IRMS). The raw data were corrected for liquid-gas fractionation and mass bias using in-house standards (Table 1). DIC concentration and isotopic composition are reported respectively in µmol.kg^{-1} and delta notation ($\delta^{13}C$-DIC) in per mil (‰) on the V-PDB scale.

Table 1: Certified Reference Materials (CRM) and in-house standards used for $\delta^{13}C$ measurements. $\delta^{13}C$ of CRM are certified by the International Atomic Energy Agency (IAEA) and Schimmelmann, et al. [34]

Standard description	Nature	Analysis	$\delta^{13}C$(‰)	SD
IAEA-CH_6	Sucrose ($C_{12}H_{22}O_{11}$)	$\delta^{13}C$-POC	-10.45	0.03
IAEA-600	Caffeine ($C_8H_{10}N_4O_2$)	$\delta^{13}C$-POC	-27.77	0.04
Acetanilide	Acetanilide (C_8H_9NO)	$\delta^{13}C$-POC	+29.53	0.01
CA21 (in-house)	Calcium carbonate ($CaCO_3$)	$\delta^{13}C$-DIC	+1,48	
Na_2CO_3 (in-house)	Sodium carbonate	$\delta^{13}C$-DIC	-6,88	
$NaHCO_3$ (in-house)	Sodium bicarbonate	$\delta^{13}C$-DIC	-5,93	
14:0 (methyl ester)	Tetradecanoic acid methyl ester	$\delta^{13}C$-FA	-29.98	0.02
14:0 (ethyl ester)	Tetradecanoic acid ethyl ester	$\delta^{13}C$-FA	-29.13	0.03
16:0 (methyl ester)	Hexadecanoic acid methyl ester	$\delta^{13}C$-FA	-29.90	0.03
16:0 (ethyl ester)	Hexadecanoic acid ethyl ester	$\delta^{13}C$-FA	-30.92	0.02
18:0 (methyl ester)	Octadecanoic acid methyl ester	$\delta^{13}C$-FA	-23.24	0.01
18:0 (ethyl ester)	Octadecanoic acid ethyl ester	$\delta^{13}C$-FA	-28.22	0.01
20:0 (methyl ester)	Icosanoic acid methyl ester	$\delta^{13}C$-FA	-30.68	0.02
20:0 (ethyl ester)	Icosanoic acid ethyl ester	$\delta^{13}C$-FA	-26.10	0.03

2.5.1. Calculation of CO_2 concentration and $\delta^{13}C$-CO_2

In addition to measured parameters, concentrations of DIC species (CO_2 and HCO_3^-) and the isotopic composition of CO_2 ($\delta^{13}C$-CO_2) were obtained by calculation. Concentrations of CO_2 and HCO_3^- were estimated using DIC concentrations, pH, temperature, and salinity via the program CO2.SYS [35] adapted for Excel.

The $\delta^{13}C$-CO_2 was calculated according to Rau, et al. [36] using $\delta^{13}C$-DIC (measured or estimated) and absolute temperature (T_k = 292 K), which was maintained constant during the experiment [36] as follows:

$$\delta^{13}C - CO_2 = \delta^{13}C - DIC + 23.644 - \frac{9701.5}{T_K} \qquad (2)$$

a. *Carbon isotope fractionation factor between bulk POC and CO_2*

The fractionation factor (ε_P) between aqueous CO_2 and POC was calculated according to Freeman and Hayes [37]:

$$\varepsilon_P = \frac{(\delta^{13}C-CO_2)-(\delta 13C-POC)}{1+\frac{(\delta 13C-POC)}{1000}} \qquad (3)$$

We performed two estimates of ε_P, with two distinct values of $\delta^{13}C$-CO_2. The first one ($\varepsilon_{P,M}$) was based on the measured values of $\delta^{13}C$-DIC in the culture medium and the corresponding $\delta^{13}C$-CO_2 calculated using Eq. 2.

The second value ($\varepsilon_{P,TA}$) was based on the isotopic composition of total assimilated DIC ($\delta^{13}C$-DIC_{TA}) estimated using a mass balance approach. This mass balance approach was motivated by the high levels of biomass (and of POC) that developed due to the external CO_2 supply and which, largely exceeded the initial DIC levels of the natural seawater used for preparing the culture. The isotopic composition of total assimilated DIC ($\delta^{13}C$-DIC_{TA}) was estimated conservatively by considering a binary mixing model between the initial DIC stock present in the natural seawater used for preparing the culture (DIC_{SW}) as the first end-member, and the added DIC due to petrochemical CO_2 addition (DIC_{petro}) as second end-member as follows:

$$(\delta^{13}C - DIC_{TA}) = f_{DIC,petro} \times (\delta^{13}C - DIC_{petro}) + (1 - f_{DIC,petro}) \times (\delta^{13}C - DIC_{SW}) \qquad (4)$$

With $\delta^{13}C$-DIC_{SW}, the isotopic composition of the initial seawater measured at day 0 and $\delta^{13}C$-DIC_{petro} the isotopic composition of DIC deriving from petrochemical CO_2 addition after gas and acid-base equilibration. For $\delta^{13}C$-DIC_{petro}, the $\delta^{13}C$-DIC measured at the end of the experiment (after 24 days of continuous CO_2 addition)

was assumed to be representative of this end-member. The $f_{DIC,petro}$, the molar fraction of petrochemical DIC assimilated by the algae, was estimated using a POC mass balance:

$$f_{DIC,petro} = \frac{([POC]_i - [POC]_0) - [DIC]_0}{[POC]_i - [POC]_0} \quad (5)$$

With $[POC]_i$ and $[POC]_0$, the respective POC concentrations at the time i and 0 and $[DIC]_0$ the initial DIC concentration before CO_2 addition.

2.5.2. Cell and POC growth rates

Algal growth rates were estimated for the exponential growth phase using two different parameters: from the cell concentrations according to Salvesen, et al. [38] and noted μ_{cell} and from the POC and noted μ_{POC} [22].

$$\mu_{cell} = \frac{ln(\frac{[alg]_i}{[alg]_{i-1}})}{(t_i - t_{i-1})} \quad (6)$$

With, $[alg]_i$ the algal concentration at time i (t_i) and $[alg]_{i-1}$ algal concentration at time i-1 (t_{i-1})

$$\mu_{POC} = \frac{ln\,[POC]_{i+1} - ln\,[POC]_i}{t_{i+1} - t_i} \quad (7)$$

With $[POC]_{i+1}$ POC concentration at time i+1 (t_{i+1}) and $[POC]_i$ the POC concentration at time i (t_i).

2.6. Fatty acids analysis

2.6.1. Separation of neutral and polar lipids

Lipid extracts were separated into neutral and polar lipids following the method of Le Grand, et al. [39]. Briefly, after sonication, 3 mL of total lipid extract was evaporated with nitrogen, recovered with three washes using chloroform:methanol (final volume 1.5 mL, 98:2 v:v) and spotted at the top of a silica gel column (40 mm x 4mm, silica gel 60A 63-200 µm rehydrated with 6% H_2O, 70-230 mesh, Sigma-Aldrich, Darmstadt, Germany). The neutral lipid fraction (NL) was eluted using chloroform:methanol (10 mL 98:2 v:v) and the polar lipid fraction (PL) with methanol (20 mL). Both fractions were then collected in glass vials, and an internal standard (C23:0, 2.3 µg) was added. NL and PL fractions were then stored at -20°C until further analysis.

2.6.2. Transesterification of FAME

Using the protocol described in Mathieu-Resuge, et al. [40], fatty acids methyl esters (FAME) were transesterified. Briefly, transesterification was realized by adding 0.8 mL of H_2SO_4/methanol mixture to the lipid extract and heated at 100°C for 10 min. Hexane (0.8 ml) and distilled water saturated in hexane (1.5 mL) were

added. The aqueous phase (lower phase, MeOH-water) was deleted after two homogenization and centrifugation. The hexane phase containing FAME was washed two more times with 1.5 mL of distilled water and stored at -20°C until further analysis. Before compound-specific isotopic analysis, samples were concentrated in 100 µL vials.

2.6.3. Fatty acids analysis by Gas Chromatography Flame Ionisation Detector (GC-FID)

Analysis of FAME was performed on a Varian CP8400 gas chromatograph by two simultaneous separations on a polar column (DB-WAX: 30 m x 0.25 mm ID x 0.25 µm, Agilent, Santa Clara, CA, USA) and on an apolar column (DB-5: 30 m x 0.25 mm ID x 0.25 µm, Agilent, Santa Clara, CA, USA). The temperature program used was the following: first, an initial heating to 0 from 150°C at 50°C.min^{-1}, then to 170°C at 3.5 °C.min^{-1}, to 185°C at 1.5 °C.min^{-1}, to 225 at 2.4°C.min^{-1} and finally to 250°C at 5.5°C.min^{-1} and maintained for 15 min.

The FAME were identified by comparison of their retention time with commercial and in-house standards mixtures. FA concentrations were reported as mgC.L^{-1} and as % of total fatty acids from each lipid fraction.

2.6.4. Fatty acids compound-specific isotope analysis

Compound specific isotope analyses (CSIA) of FAME were performed using protocol by Mathieu-Resuge, et al. [40]. CSIA analyses were made on a Thermo-Fisher Scientific (Waltham, MA, USA) GC ISOLINK TRACE ULTRA using the same polar column as for FAME analysis by GC-FID (DB-WAX: 30 m x 0.25 mm ID x 0.25 µm, Agilent, Santa Clara, CA, USA). Only the 10 fatty acids with the highest concentrations (14:0, 16:0, 16:1n-7, 16:3n-4, 18:1n-9, 18:1n-7, 18:2n-6, 18:3n-6, 18:4n-3, 20:4n-6 and 20:5n-3) were selected for compound-specific isotopic analysis, the others presenting too low voltage amplitudes to allow precise stable isotope measurement (i.e amplitudes < 800 mV and concentration < 100 µgC.L^{-1}) were not considered. However, exceptions were made for three fatty acids (18:1n-9, 18:1n-7 and 16:3n-4 in the NL fraction) despite presenting amplitudes lower than 800 mV. Unfortunately, all FA attributed to bacteria were below these thresholds.

As for δ^{13}C-POC and δ^{13}C-DIC, δ^{13}C-FA was reported in delta notation (δ) expressed in per mil (‰) against V-PDB standard. Calibration to the V-PDB scale was performed using a mix of 8 acid ethyl and methyl esters (14:0, 16:0, 18:0 and 20:0, with δ^{13}C-FA values ranging from − 26.98 ± 0.02‰ to − 30.38 ± 0.02‰) and supplied by Indiana University Stable Isotope Reference Materials as described in Mathieu-Resuge, et al. [40]

(Table 1). The analytical error and analytical precision were 0.2‰ and <0.2‰, respectively, as previously measured by Mathieu-Resuge, et al. [40]. Accordingly, the standards were run at the start of the analytical sequence and also after every three samples for quality control and isotope correction of fatty acid isotopic signature in samples.

2.6.5. Correction of δ^{13}C-FA due to trans-esterification

Corrections of δ^{13}C-FA values have been made according to the method described in Mathieu-Resuge, et al. [40] and using the following equation:

$$(\delta^{13}Cmethanol) = -n \times (\delta^{13}CFA) + (n+1) \times (\delta^{13}CFAME) \quad (8)$$

Where n is the number of carbon atoms in the free FA. The average δ^{13}C–methanol value used in this correction (-39.6‰) was estimated by Mathieu-Resuge, et al. [40].

2.6.6. Comparison of fatty acids isotopic composition with bulk POC

To compare fatty acid isotopic composition (δ^{13}C-FA) and POC isotopic composition (δ^{13}C-POC), we defined $\Delta_{FA\text{-}POC}$ as follow:

$$\Delta_{FA-POC} = \delta^{13}CFA - \delta^{13}CPOC \quad (9)$$

2.6.7. Isotopic composition of classes of fatty acids and total fatty acids

Weighted average carbon isotopic signatures ($\delta^{13}C\text{-}FA_{WA}$) were calculated for the different classes of fatty acids (SFA, MUFA, PUFA) as well as n-3 and n-6 PUFA and total neutral lipids (TNL) and total polar lipids (TPL) using the following equation

$$(\delta^{13}CFA_{WA}) = \frac{\sum_i^n (\delta^{13}CFA_i) \times [FA]_i)}{\sum_i^n [FA]i} \quad (10)$$

Where $\delta^{13}C\text{-}FA_i$ and $[FA]_i$ are the isotopic composition and massic concentration ($mgC.L^{-1}$) of fatty acid i.

2.6.8. Statistical analysis

To assess the potential effect of time and difference between replicates during algae development, ANOVA or PERMANOVA analysis had been conducted on the FA mass percentages separately in NL and PL, FA isotopic composition and $\Delta_{FA\text{-}POC}$. Principal component analysis (PCA) coupled with similarity percentage analysis (SIMPER) was made to identify fatty acids that were the main responsible for the overall observed variability (80%). Spearman test was also conducted on fatty acids abundance in both PL and NL to explore the

relationship between fatty acids. Pairwise Student tests were used to compare isotopic composition between lipid fraction and between FA. All statistical analyses were performed using R software [41].

3. RESULTS

3.1. Growth parameters

The growth of *Chaetoceros muelleri* has been divided into 3 phases according to cell abundance/concentration (Figure 1): (i) an initial and exponential growth phase from t_0 to t_5 (Phase I), (ii) a stationary phase between t_5 and t_{14} (Phase II) and finally (iii) a decline phase from t_{14} until the end (t_{24}) (Phase III). During Phase I, cell concentration increased rapidly (Figure 1A), from 7.3 x 10^4 to 1.2 x 10^7 cells.mL^{-1} on average for the three replicates corresponding to a mean cellular growth rate of 0.44 d^{-1} (doubling time 1.56 d).

During Phase II, cell concentration remained high and relatively stable, around 1.30 x 10^7 cells.mL^{-1} until t_{14}. After t_{14} (Phase III), cell concentration decreased down to 9 x 10^6 cells.mL^{-1} with a concomitant increase in bacteria concentration. Bacteria concentration was, on average, three times higher than algal cell concentration during Phase I and around 17 times higher during Phase III (Figure 1B).

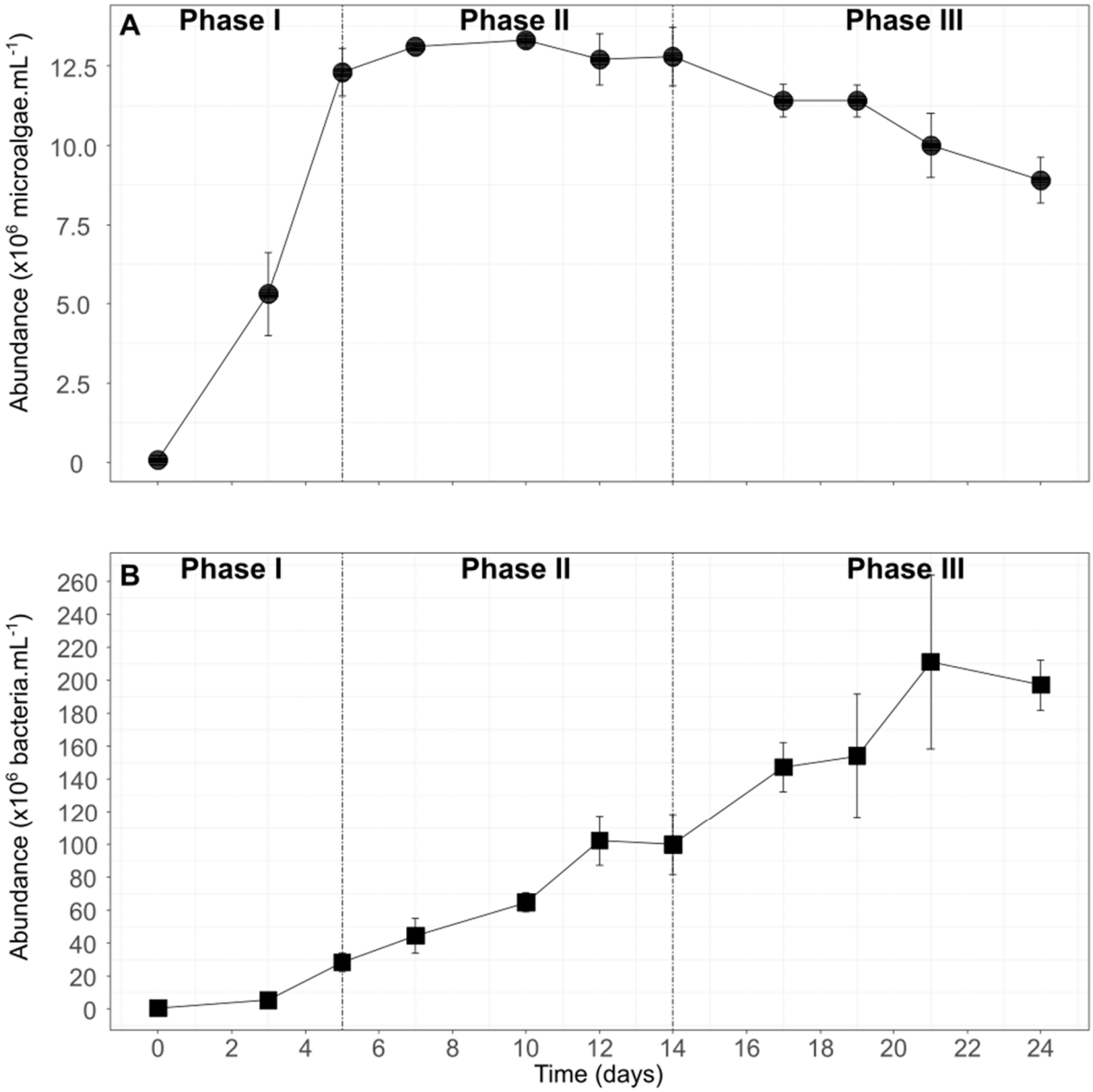

Figure 1: Growth of *Chaetoceros muelleri* (●) [A] and associated bacterial development (■) [B]. The vertical lines define the different growth phases of *C. muelleri*: Phase I (t_0-t_5), Phase II (t_5-t_{14}), Phase III (t_{14}-t_{24}). The standard deviations (± SD) show the variability between culture replicates (n=3).

3.2. Physiological parameters

Cell size and complexity (estimated from FSC and SSC) decreased from 93 to 74 a.u and 22 to 9 a.u, respectively, during the first five days (Phase I) and then rose slowly to 82 a.u and 17 a.u respectively till day 14 (Phase II). During Phase III (day 14 till day 23), FSC ranged between 62 and 83 a.u. and SCC between 12 and 19 a.u. (Table 2). Cell viability remained high between 92 and 97% for the whole duration of the culture (Table 2).

Chlorophyll content (FL3 fluorescence) decreased during the entire experiment from 25 to 7 a.u. The largest decline occurred during the exponential growth phase between t_0 and t_3 (a decline of 10 a.u). The highest NL content estimated by BODIPY staining (green fluorescence on FL1) was observed during Phase II at t_{19} with 473 a.u. while the lowest value was visible during Phase I (in average 110 a.u) (Figure 2).

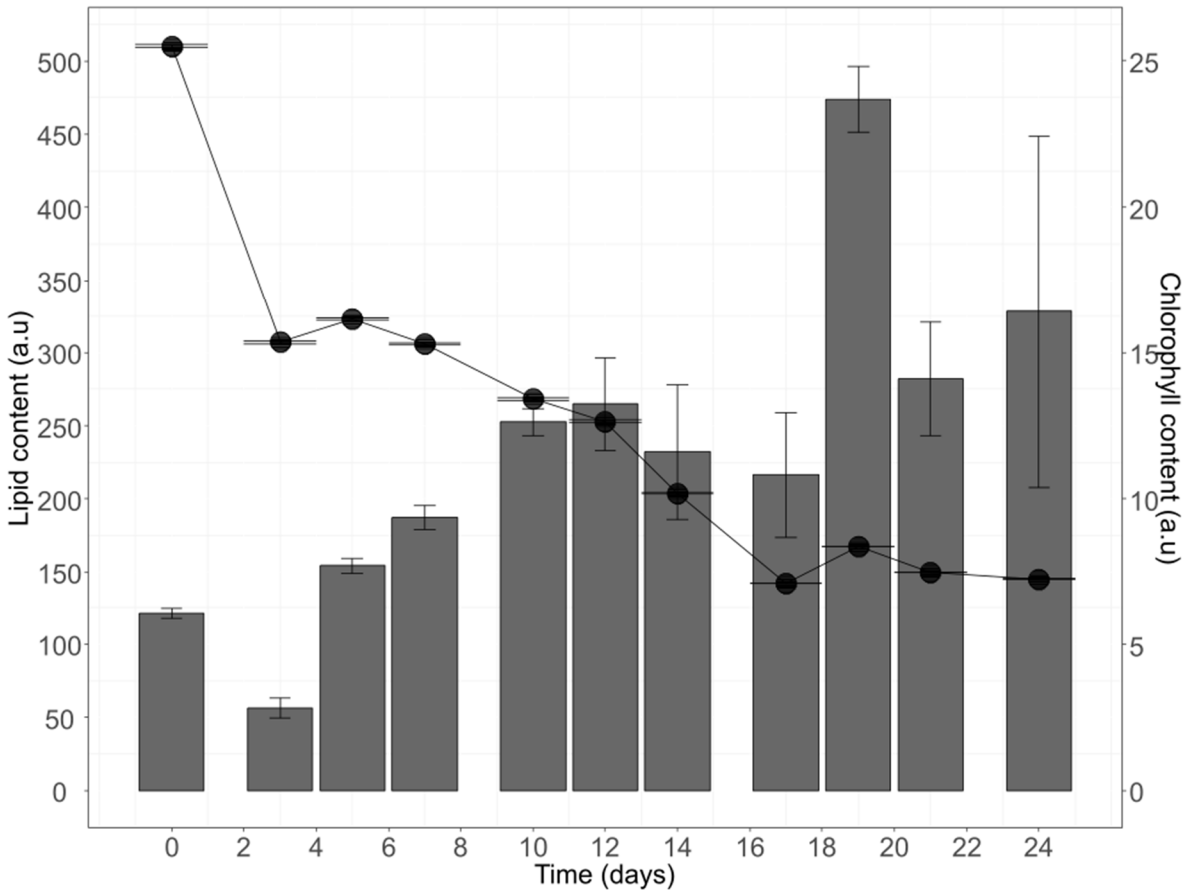

Figure 2: Temporal dynamics of NL lipid content (estimated by BODIPY staining, barplot) and chlorophyll content as proximate by FL3 fluorescence (line plot). Error bars refer to standard deviations (± SD) between culture replicates (n=3).

Table 2: Temporal dynamics of *C. muelleri* morphological and viability parameters during culture. Results are expressed as Mean ± SD (n=3). FSC=Forward Scatter; SSC=Side Scatter

Time (days)	FSC	SSC	% of live cells
0	93.07 ± 2.63	21.69 ± 2.21	91.91 ± 2.00
3	64.23 ± 1.19	6.93 ± 0.21	94.39 ± 3.14
5	74.22 ± 1.54	9.03 ± 0.39	97.23 ± 1.09
7	77.43 ± 1.69	11.71 ± 0.05	96.94 ± 1.83
10	79.83 ± 1.95	14.19 ± 0.17	96.68 ± 2.48

12	81.00 ± 2.23	15.78 ± 0.14	96.48 ± 2.20
14	82.94 ± 2.29	17.01 ± 0.26	96.79 ± 1.96
17	62.56 ± 1.32	12.90 ± 0.30	94.43 ± 2.23
19	68.41 ± 1.03	15.88 ± 0.31	96.55 ± 2.09
21	45.06 ± 0.83	12.78 ± 0.27	96.74 ± 2.01
24	68.52 ± 0.61	19.57 ± 0.19	96.27 ± 2.07

3.3. Dissolved inorganic carbon (DIC) concentration and isotopic composition

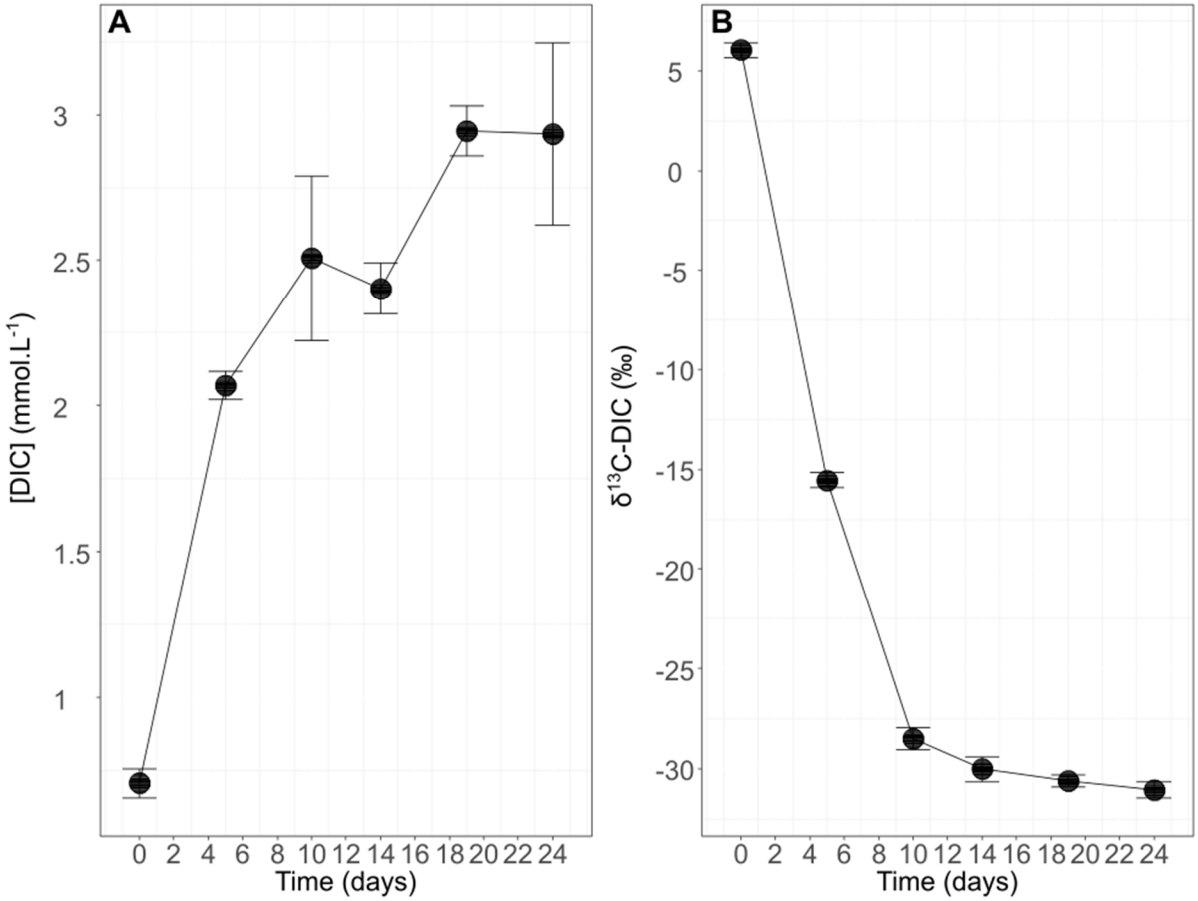

Figure 3: Temporal dynamics of DIC concentration [A] and isotopic composition [B] of *C. muelleri*. Results are expressed as mean ± SD (n=3)

DIC concentration increased from 0.7 to 2.9 mmol.L^{-1} during the 24 days of the experiment. The final DIC concentration tended to reach a plateau of around 2.9 mmol.L^{-1} (Figure 3A). δ^{13}C-DIC decreased rapidly during the exponential growth phase (Phase I) from 6.0‰ to -15.5‰, then stabilized at -29.3‰ during phases II and III (Figure 3B).

3.4. Particulate organic carbon (POC) concentration and isotopic composition

During Phase I, POC concentrations increased rapidly from 1.5 to 22.0 mmol.L^{-1} (Figure 4A) and reached a plateau during Phase III around 22.3 mmol.L^{-1}. δ^{13}C-POC also showed variations during the culture with a rapid and consistent decrease during Phase I of 36‰ in 5 days from -12.9‰ to -48.7‰ (Figure 4B). During Phases II and III, *C. muelleri* isotopic composition kept decreasing and reached a minimum value of -57.0‰ at t_{24}. The carbon quota of the cell (i.e., the C content per cell) decreased first during Phase I. It then increased continuously afterward from t_5 to t_{24}, indicating a progressive accumulation of organic carbon into cells. Algae cells exhibited a mean final C quota of 2.4 pmolC.cells^{-1} (Figure 4C).

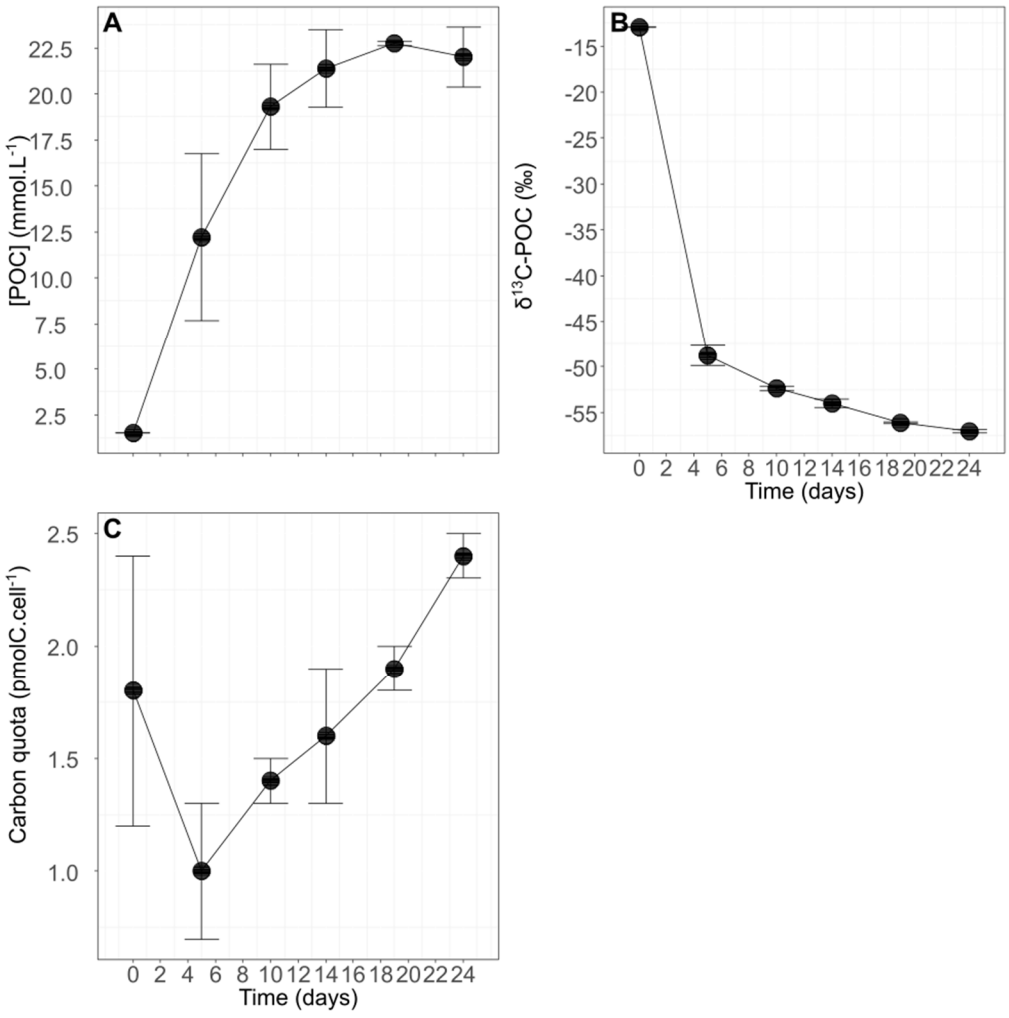

Figure 4: Dynamics of POC concentrations [A], POC isotopic composition [B] and carbon quota [C] for *C. muelleri*. Results are expressed as Mean ± SD (n=3)

3.5. Isotopic fractionation between CO_2 and bulk POC

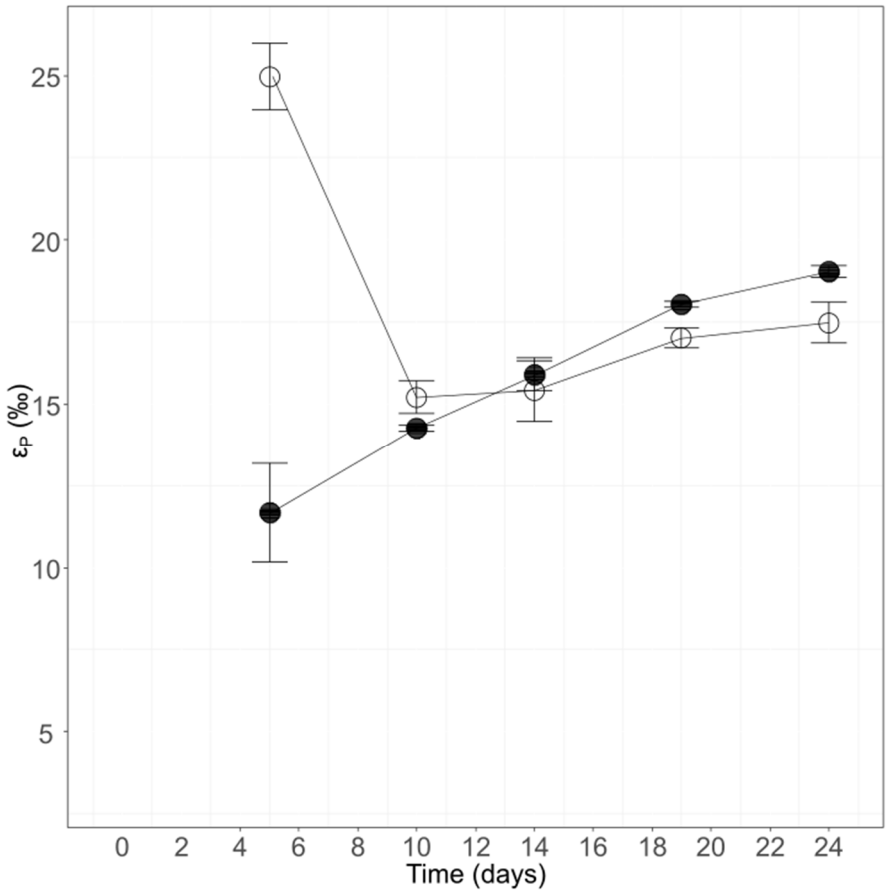

Figure 5: Temporal dynamics of isotopic fractionation between CO_2 and bulk POC deduced from measurement and total assimilated DIC (respectively $\varepsilon_{P,M}$ (solid line white dot) and $\varepsilon_{P,TA}$ (solid line black dot). Results are expressed as Mean ± SD (n=3).

Fractionation factors (ε_P) varied during the experiment and substantially according to the $\delta^{13}C$-CO_2 chosen as reference (Figure 5). The highest value (24.9‰) was observed for $\varepsilon_{P,M,}$ at the end of Phase I (t_5). Then, it decreased during Phase II (mean value of 15.3‰) and finally slightly increased during Phase III to reach 17.2‰. The fractionation factor calculated versus total assimilated DIC ($\varepsilon_{P,TA}$) was 11.7‰ at the end of Phase I. Then, it presented a similar temporal dynamic to $\varepsilon_{P,M}$, increasing steadily during Phases II and III reaching 19.0‰. Fractionation factor versus total assimilated DIC ($\varepsilon_{P,TA}$) was negatively correlated to the ratio FSC/SSC and chlorophyll content (linear models: $R^2 > 0.94$, $p < 0.001$ for both correlations) (Figure 6).

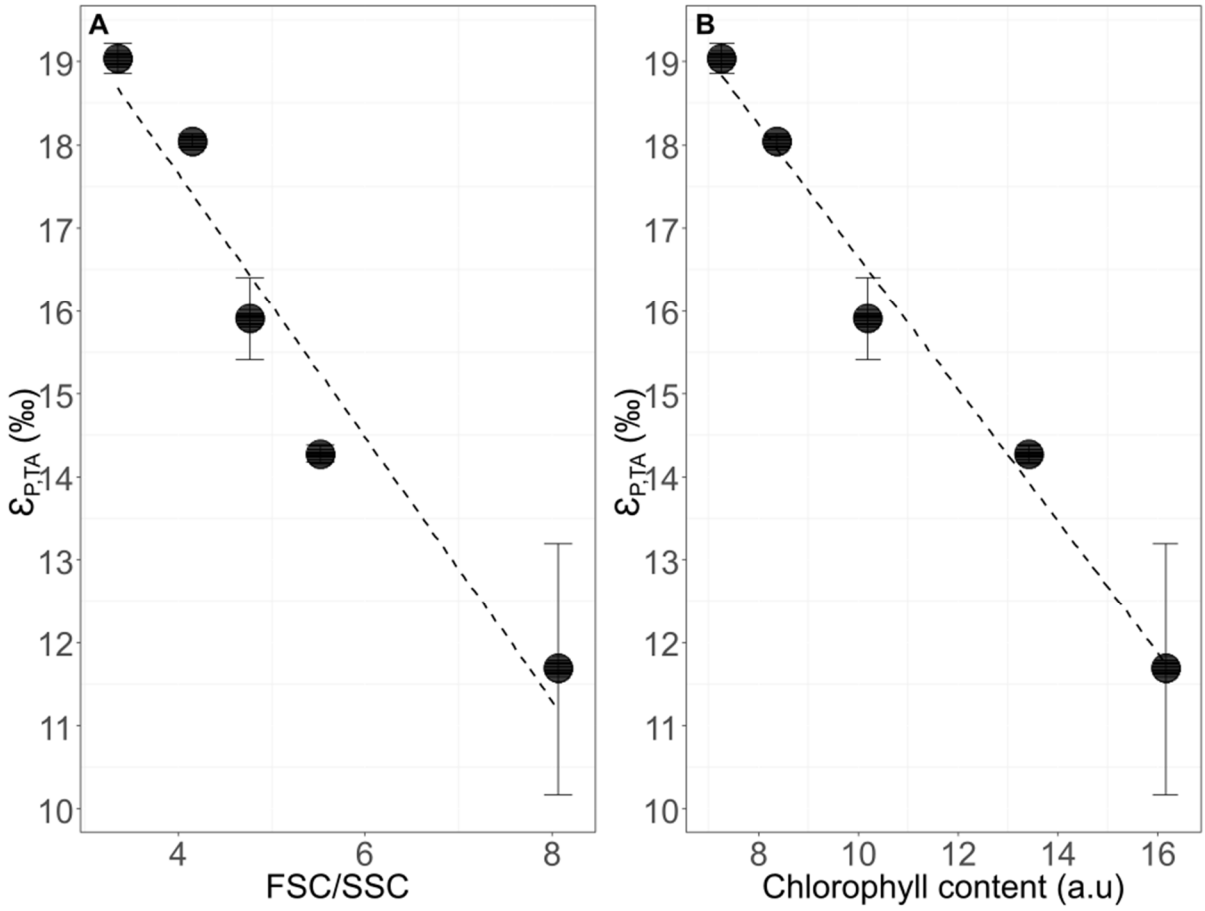

Figure 6: Correlations of isotopic fractionation calculated versus total assimilated DIC ($\varepsilon_{P,TA}$) with FSC/SSC ratio ($\varepsilon_{P,TA}$ = 24-1.6*FSC/SSC R^2=0.94 $p < 0.001$) [A], and with chlorophyll content ($\varepsilon_{P,TA}$ =25 – 0.8*Chla R^2=0.98 $p < 0.001$) [B].

3.6. Content and percentage of fatty acids in neutral and polar lipid fractions.

A total of 50 FA have been identified, with 35 of them being in low amounts (less than 1% of the total fatty acids). Total fatty acids (TFA) in neutral lipid fraction (TNL) varied between0.8 ± 0.04 mg.L^{-1} at t_0 to 66.3 ± 8.9 mg.L^{-1} at t_{14}). In comparison, total fatty acids in polar lipid fraction (TPL) increased from 3.2 ± 0.2 mg.L^{-1} to 17.1 ± 0.6 mg.L^{-1} in Phase I (between t_0 and t_5) and then remained relatively constant between Phase I (t_5) and Phase II (t_{14}) (in average 18.1 mg.L^{-1}) (Figure 7). PL fraction was dominated by polyunsaturated fatty acids (PUFA), and their proportion relative to TFA decreased with time (from 49% at Phase I (t_5) to 37% at Phase II (t_{14}). In the NL fraction, saturated fatty acids (SFA) were the most important FA category with increasing proportion with time (43% at Phase I (t_5) to 50% at the end of Phase II (t_{14})) inversely to PUFA. In both fractions, PUFA decreased in favor of monounsaturated fatty acids (MUFA) and SFA. BACT (bacterial fatty acids) remained below 1.5% in NL and below 4% in PL between Phase I (t_5) and the end of Phase II (t_{14}) (Table

3). Interestingly, the proportion of BACT increased with time in PL (2 to 4%) and paralleled the increase of bacterial concentration, as shown in Figure 1.

For the PL and NL fractions, the primary FA were 14:0, 16:0, 16:1n-7, and 20:5n-3. As for PUFA, 20:5n-3 proportion decreased with time in both PL and NL. The highest proportions of 20:5n-3 were observed at Phase I (PL: 34% and NL: 9.4%) (Table 3).

Table 3: Relative proportions (in %) of the primary fatty acids (>1% of TFA) of *Chaetoceros muelleri*. TFA represents the sum of all fatty acids and includes saturated fatty acids (SFA), monounsaturated fatty acids (MUFA), polyunsaturated fatty acids (PUFA) and bacterial fatty acids (BACT FA). Results are expressed as Mean ± SD (n=3).

	Phase I				**Phase II**			
Time (d)	**t_0**		**t_5**		**t_{10}**		**t_{14}**	
Fraction	**NL**	**PL**	**NL**	**PL**	**NL**	**PL**	**NL**	**PL**
14:0	25.7 ± 0.1	15.8 ± 0.4	24.1 ± 3.5	17.1 ± 0.7	16.7 ± 0.3	14.9 ± 0.8	16.0 ± 0.2	13.7 ± 0.1
16:0	12.0 ± 0.1	3.3 ± 0.0	17.6 ± 10.6	10.5 ± 0.9	31.1 ± 0.6	15.1 ± 0.1	33.1 ± 0.2	16.5 ± 0.6
18:0	2.0 ± 0.1	0.9 ± 0.0	0.6 ± 0.1	0.6 ± 0.0	0.5 ± 0.0	1.3 ± 0.0	0.6 ± 0.0	2.3 ± 0.0
16:1n-7	20.0 ± 0.1	11.2 ± 0.1	33.0 ± 3.9	17.7 ± 0.3	34.2 ± 0.2	21.2 ± 0.1	34.1 ± 0.2	21.1 ± 0.4
18:1n-9	0.9 ± 0.1	1.5 ± 0.0	0.7 ± 0.1	1.3 ± 0.1	0.5 ± 0.0	2.3 ± 0.1	0.5 ± 0.0	3.3 ± 0.1
18:1n-7	0.4 ± 0.1	4.5 ± 0.0	0.2 ± 0.0	1.5 ± 0.2	0.3 ± 0.0	2.8 ± 0.2	0.4 ± 0.0	3.5 ± 0.2
16:2n-7	1.8 ± 0.1	2.8 ± 0.0	1.4 ± 0.3	1.3 ± 1.1	0.4 ± 0.0	1.0 ± 0.1	0.3 ± 0.1	0.7 ± 0.0
16:2n-4	1.8 ± 0.1	2.3 ± 0.0	0.6 ± 0.1	1.4 ± 0.0	0.6 ± 0.0	1.3 ± 0.1	0.6 ± 0.0	1.1 ± 0.1
16:3n-4	2.5 ± 0.1	11.1 ± 0.0	0.7 ± 0.1	6.0 ± 0.3	0.7 ± 0.0	3.2 ± 0.0	0.6 ± 0.0	2.3 ± 0.1
18:2n-6	0.9 ± 0.0	1.4 ± 0.0	1.7 ± 0.3	3.0 ± 0.2	1.3 ± 0.0	3.2 ± 0.0	1.3 ± 0.0	3.4 ± 0.1
18:3n-6	0.4 ± 0.0	0.5 ± 0.0	1.3 ± 0.2	2.3 ± 0.3	1.3 ± 0.0	2.5 ± 0.2	1.1 ± 0.0	2.2 ± 0.1
18:4n-3	1.0 ± 0.0	1.1 ± 0.0	1.3 ± 0.2	2.0 ± 0.1	1.3 ± 0.1	2.0 ± 0.2	1.2 ± 0.1	2.2 ± 0.1
20:4n-6	0.6 ± 0.0	0.9 ± 0.0	1.9 ± 0.3	3.7 ± 0.2	2.0 ± 0.0	3.9 ± 0.1	1.7 ± 0.0	3.3 ± 0.1
20:5n-3	9.4 ± 0.0	34.1 ± 0.4	10.1 ± 1.3	26.2 ± 1.0	6.6 ± 0.0	20.0 ± 0.4	6.0 ± 0.1	18.3 ± 0.5
22:6n-3	0.6 ± 0.0	2.2 ± 0.0	0.5 ± 0.1	2.3 ± 0.0	0.5 ± 0.0	2.0 ± 0.1	0.5 ± 0.0	2.3 ± 0.1
SFA	**41.2 ± 0.0**	**20.7 ± 0.5**	**43.2 ± 7.0**	**28.9 ± 1.3**	**48.8 ± 0.3**	**32.6 ± 1.1**	**50.3 ± 0.2**	**34.0 ± 1.0**
MUFA	**31.0 ± 0.6**	**19.8 ± 0.1**	**35.7 ± 4.2**	**21.4 ± 0.5**	**35.9 ± 0.2**	**26.8 ± 0.3**	**35.6 ± 0.1**	**28.6 ± 0.5**

PUFA	**23.1 ± 1.2**	**58.9 ± 0.6**	**20.5 ± 2.9**	**49.5 ± 1.6**	**15.2 ± 0.0**	**40.5 ± 0.9**	**14.0 ± 0.2**	**37.3 ± 0.7**
BACT	**8.3 ± 0.0**	**5.8 ± 0.0**	**1.5 ± 0.1**	**2.1 ± 0.2**	**0.7 ± 0.0**	**3.2 ± 0.2**	**1.0 ± 0.3**	**4.0 ± 0.2**
TOTAL ($mgC.L^{-1}$)	**0.8 ± 0.0**	**3.2 ± 0.2**	**20.8 ± 4.8**	**17.1 ± 0.6**	**52.2 ± 0.8**	**18.7 ± 0.8**	**66.3 ± 8.9**	**18.7 ± 0.6**

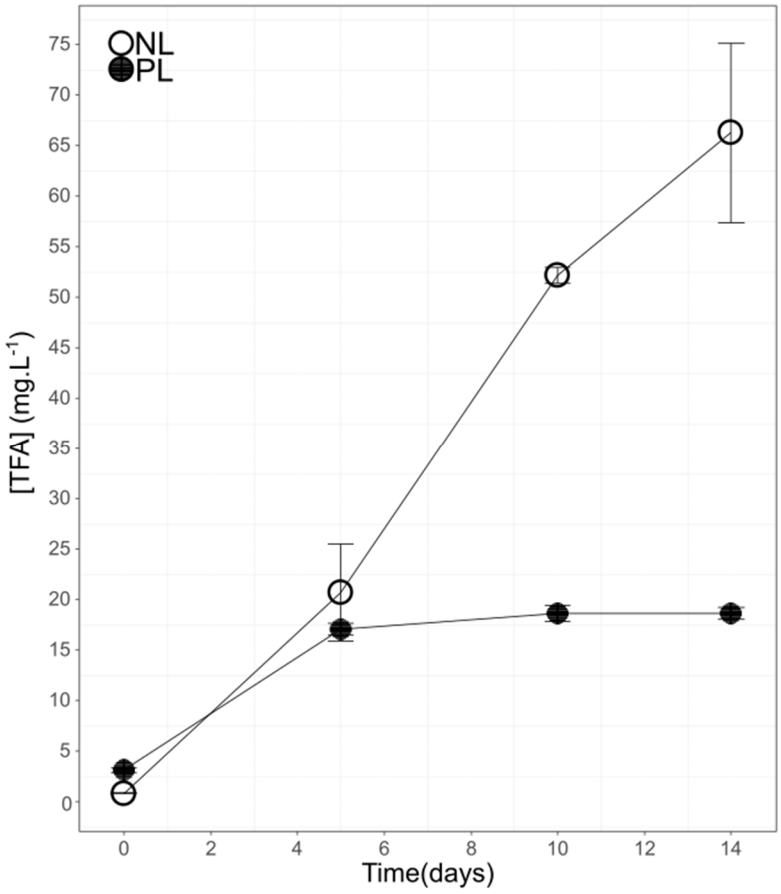

Figure 7: Temporal dynamics of total fatty acids (TFA) concentrations (in $mg.L^{-1}$) for *Chaetoceros muelleri* for both neutral (NL – white dots) and polar (PL – black dots) lipid fractions. Results are expressed as Mean ± SD (n=3).

The PERMANOVA analysis conducted on NL and PL fatty acids during Phase 1 (t_5) and Phase II (t_{10} and t_{14}) revealed a significant difference between sampling times (t_5, t_{10}, t_{14}) for fatty acid percentage ($p < 0.001$) but no significant difference between cultures replicates ($p > 0.05$).

The PCA conducted for total fatty acids and coupled with SIMPER analysis showed a clear difference between culture phases. The first sampling points (t_5 and t_{10}) were located on the negative side of axis 1 while the last sampling points (t_{14}) were on the positive side (Figure 8). Axis 1 was driven on the positive side by fatty acids 14:0, 16:3n-4 and 20:5n-3 and on the negative side by 16:0, 16:1n-7 and 18:1n-9. These fatty acids

presented opposite proportion dynamics in PL (increases for 16:0, 16:1n-7 and 18:1n-9 and decreases for 14:0, 16:3n-4 and 20:5n-3) (Table 3). Axis 2 was related to lower proportion fatty acids such as 22:6n-3 and 18:2n-6 (positive side) and 20:4n-6 and 18:3n-6 (negative side) in lower proportions (Figure 8). 16:0 and 16:1n-7 appeared to be significantly and positively correlated (Spearman test: TFA: $\alpha = 0.94$ p-value < 0.0001, PL: $\alpha = 0.87$ p-value < 0.0001 and NL: $\alpha = 0.93$ p-value < 0.0001), as well as 16:3n-4 and 20:5n-3 (Spearman test: TFA: $\alpha = 0.92$ p-value < 0.0001 and PL: $\alpha = 0.85$ p-value < 0.0001) and 18:3n-6 and 20:4n-6 (Spearman test: TFA: $\alpha = 0.95$ p-value < 0.0001, PL: $\alpha = 0.88$ p-value < 0.0001 and NL: $\alpha = 0.89$ p-value < 0.0001), and finally 20:5n-3 and 14:0 (Spearman test: NL: $\alpha = 0.96$ p-value < 0.0001)

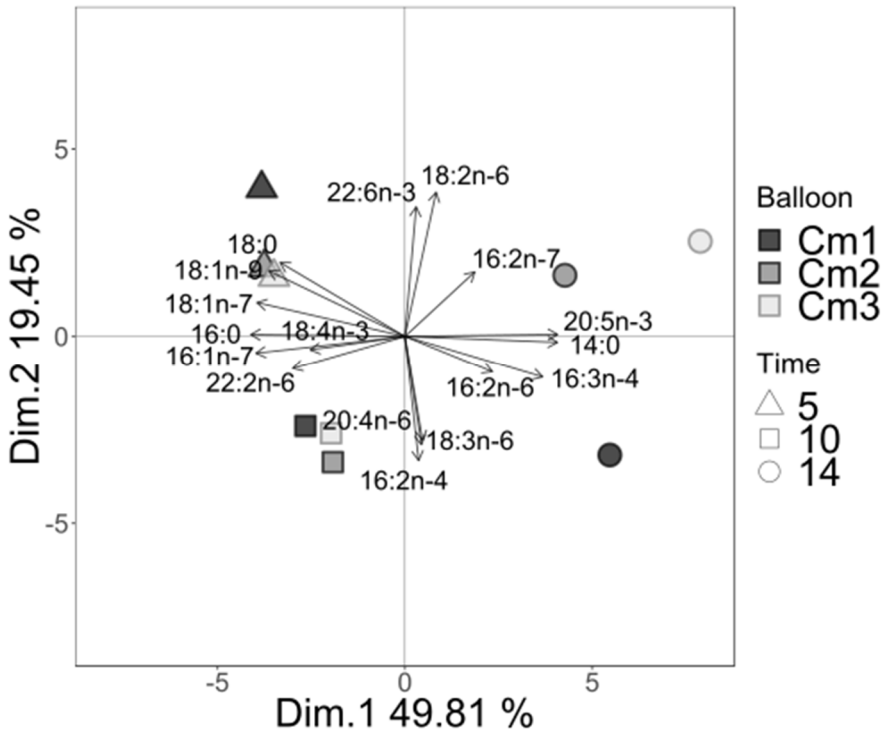

Figure 8: Principal component analysis (PCA) made with % of total fatty acids. Only the FA selected by SIMPER analysis are shown here (explaining 80% of the variability). The colors represent the different culture replicates, and the symbol shapes the sampling times. (Cm = *Chaetoceros muelleri*, n=9)

3.7. Carbon isotopic composition of fatty acids

Carbon isotopic composition (δ^{13}C-FA) for the 11 FA studied are available in Figure 9A. In general, δ^{13}C-FA decreased with time (from -52.9 ± 1.5‰ at t_5 to -58.2 ± 1.1‰ at t_{14} in average for NL (ANOVA: p-value < 0.001) and from -54.1 ± 2.6‰ to -57.2 ± 1.6‰ in average for PL (PERMANOVA: p-value < 0.01) (Table 4). δ^{13}C-FA of lipid classes (SFA, MUFA, and n-6 PUFA) also showed a substantial decrease during the experiment for both NL and PL fractions while for n-3 PUFA it was more stable. During Phase I (t_5), δ^{13}C-SFA are lower in

comparison with δ^{13}C-PUFA (Table 4). Overall, the difference between FA categories attenuated with aging culture ranging from -52‰ to -57‰ at t_5 and from -56‰ to 58.6‰ at t_{14}, During Phase I, δ^{13}C of n-3 PUFA were also lighter than δ^{13}C of n-6 PUFA (Table 4). δ^{13}C of 18:2n-6, 18:3n-6 and 18:4n-3 in the PL fraction were always significantly lower than the NL fraction (pairwise Student test, p-value < 0.05) while it was the contrary for 14:0, 16:0 and 20:4n-6 (pairwise Student test, p-value < 0.05). Isotopic compositions of 16:1n-7, 16:3n-4, and 20:5n-3 in the PL fraction were not significantly different from their isotopic signatures in the NL fraction (pairwise Student test, p-value > 0.05). For the PL fraction, highest δ^{13}C-FA were observed at t_5 for C_{18} fatty acids (18:1n-9: -50.8 ± 0.2 ‰, 18:2n-6: -51.6 ± 0.1 ‰, 18:3n-6: -51.0 ± 0.7 ‰ and 18:1n-7: -52.0 ± 0.2 ‰) and 16:0 (-51.3 ± 0.2 ‰). At t_{14} 16:0 and 18:4n-3 were most ^{13}C depleted (respectively -58.8 ± 0.0 ‰ and -59.1 ± 0.0 ‰). Regarding the NL fraction, 16:0 and 16:1n-7 were both the least depleted in ^{13}C at t_5 (respectively -51.8 ± 0.4 ‰ and -52.6 ± 0.1 ‰) and the most depleted in ^{13}C at t_{14} (respectively -59.3 ± 0.4 ‰ and -58.1 ± 0.6 ‰).

Table 4: Time variation of weighted average carbon isotopic composition for each lipid class (SFA, MUFA, PUFA) as well as n-3, n-6 PUFA measured for neutral (NL) and polar (PL) fractions. Results are expressed as Mean ± SD (n=3)

Phase	**Phase I**				**Phase II**							
Time (d)	**5**				**10**				**14**			
Fraction	**NL**		**PL**		**NL**		**PL**		**NL**		**PL**	
(‰)	**ȳ**	**sd**	**ȳ**	**sd**	**ȳ**	**sd**	**ȳ**	**sd**	**ȳ**	**sd**	**ȳ**	**sd**
SFA	-52.2	0.4	-52.7	1.2	-56.8	1.0	-56.2	1.4	-58.6	1.1	-57.7	1.7
MUFA	-52.6[1]	0.3	-52.0	0.4	-56.4[1]	0.6	-55.3	1.1	-58.1[1]	0.6	-57.0	1.6
PUFA	-55.4[1]	2.0	-56.0	2.4	-55.5	0.9	-56.0	1.2	-56.4	1.1	-56.6	1.3
n-3	-56.4	0.9	-56.9	0.3	-55.5	0.5	-56.0	0.5	-55.9	0.9	-56.2	1.1
n-6	-52.8	0.2	-51.7	0.7	-55.3	0.9	-55.8	1.5	-57.2	0.9	-57.8	1.3
TOTAL	**-52.9[1]**	**1.5**	**-54.1**	**2.6**	**-56.5[1]**	**0.9**	**-55.9**	**1.2**	**-58.2[1]**	**1.1**	**-57.2**	**1.6**

[1]: weighted averages calculated despite lower signal on GC-c-IRMS (< 800 mV) for 18:1n-9, 18:1n-7 & 16:3n-4 (in NL)

The dynamics of 16:3n-4, 18:4n-3 and 20:5n-3 isotopic compositions were overall more stable than other of the FA. 16:3n-4 isotopic composition in both fractions tended to remain relatively stable (-57.4 ± 0.2 ‰ in NL and -58.6 ± 0.2 ‰ in PL). The same observations could be made for 20:5n-3 with, however, a slightly increasing

trend between t_5 and t_{10} (average isotopic composition over the studied period: -56.1 ± 0.6 ‰). In NL, 18:4n-3 isotopic signature was progressively more depleted in ^{13}C while in PL fraction, its isotopic composition was close to 20:5n-3 at t_5 and t_{10}. Then, 18:4n-3 isotopic composition decreased by 3‰ in PL and by 2‰ in NL between t_{10} and t_{14}.

Isotopic compositions of 16:3n-4 (NL) and 16:1n-7 (PL) as well as 16:3n-4 (PL) and 16:1n-7 (NL) tended to become similar at the end of the monitoring (respectively -58.3 ± 0.2 ‰ and -57.4 ± 0.2 ‰). Similar observations can be made at t_{14} for 20:4n-6 (PL and NL) and 20:5n-3 (PL) (averaging at -56.3 ± 0.2 ‰). After t_5, 20:4n-6 was always less depleted in ^{13}C than C_{18} PUFA (18:2n-6, 18:3n-6 and 18:4n-3) in both fractions.

Figure 9B compares the isotopic composition of POC and those of FA. For the 11 fatty acids studied, $\Delta_{FA\text{-}POC}$ were all negative (except 18:1n-9 and 18:1n-7 in PL at t_{14}) corresponding to a ^{13}C-depletion in all FA in comparison with POC for both PL and NL. The largest ^{13}C difference between POC and FA was observed during exponential growth phase (at t_5) for 16:3n-4 (NL: -10.8 ± 1.2 and PL: -9.7 ± 1.0), for 20:5n-3 (PL: -8.2 ± 0.9 and NL: -7.9 ± 1.0) and for 18:4n-3 (PL: -8.0 ± 1.8) while the smallest were noted for 18:1n-7, 18:1n-9 and 20:4n-6 in PL fraction at t_{14} (respectively 0.4 ± 2.0, 0.1 ± 1.2; and -1.7 ± 1.5). Difference between POC and FA isotopic composition remained relatively constant for 14:0 (NL: ANOVA p-value > 0.05), 16:1n-7 (NL and PL: both ANOVA p-value > 0.05), 18:4n-3 (NL: ANOVA p-value > 0.05), 18:2n-6 (NL: ANOVA p-value > 0.05) and 18:3n-6 (NL: ANOVA p-value > 0.05) while they increased for 16:0 in NL and PL (ANOVA p-value < 0.02 and p-value < 0.03 respectively). The difference between POC isotopic signature and those of 20:5n-3 (NL: ANOVA p-value < 0.001 and PL: ANOVA p-value < 0.001) and 16:3n-4 (NL: ANOVA p-value < 0.001 and PL: ANOVA p-value < 0.001) progressively decreased with time.

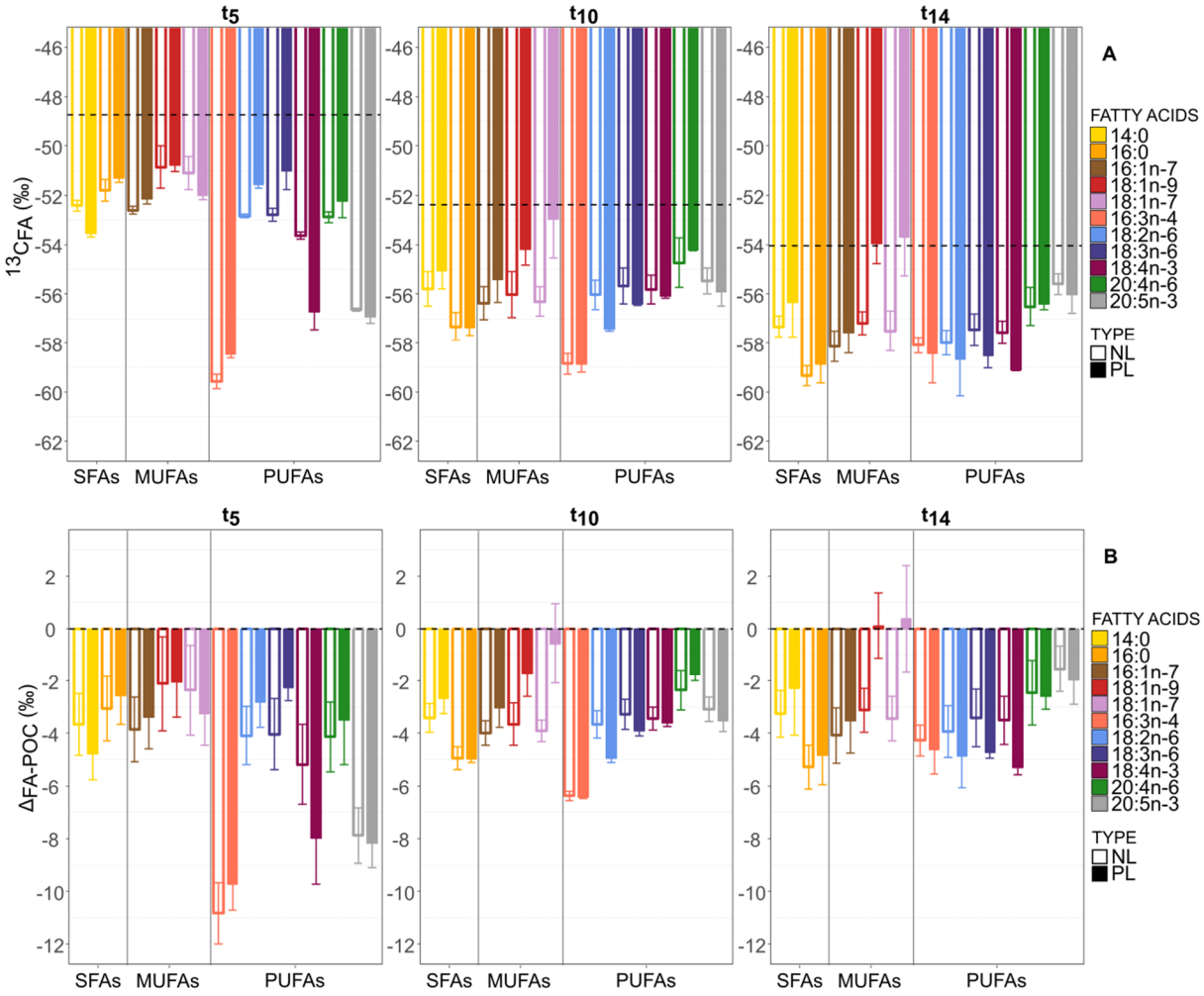

Figure 9: [A] Isotopic ratios (δ^{13}C-FA) of the eleven main fatty acids studied in *C. muelleri*. The isotopic composition of POC (dashed line) is considered here as a reference. The empty bars correspond to neutral lipids (NL) and the filled ones to polar lipids (PL). Results are expressed as Mean ± SD (n=3, and n=2 for PL fraction for fatty acids with *). [B] Comparison of POC and FA isotopic compositions ($\Delta_{FA\text{-}POC}$) in NL and PL fractions.

4. DISCUSSION

4.1. Morphological and physiological changes during *C. muelleri* culture

The cellular characteristics of marine microalgae change during growth and development. In this study, the forward scatter (FSC), and side scatter (SSC) values were more strongly impacted during the exponential phase (Phase I). This change is linked to the morphological changes occurring in *C. muelleri*, of shape, but also in its cytoplasmic characteristics or its cell surface [31]. Indeed, the size and complexity of cells tend to decrease during growth to improve the organism's fitness to its environment [42] but also in response to changing nutritional conditions. A decrease in red fluorescence (FL3 – chlorophyll content) was observed for *C. muelleri*.

This loss of chlorophyll was associated with a reduction in FSC (size) and SSC (complexity) and was accentuated during the growth phase (Phase I). This might have reflected a decrease in the efficiency of the photosynthetic apparatus. Indeed, with the large multiplication of biomass during the exponential phase (Phase I), a self-shading effect (corresponding to stress for the alga) could prevent cells from correctly capturing photons useful for their photosynthesis, thus reducing their photosynthetic efficiency [31, 43, 44]. In addition, *C. muelleri* was grown under continuous light to insure a good FA production and synthesis. George, et al. [43] have shown that cells growing under these conditions tend to be smaller and clump. This would strengthen self-shading and increase stress. In the longer term, this limitation of access to light would be a factor in stopping growth [44]. This would also explain the growth slowdown observed during Phase III by photosynthetic limitation.

4.2. Dissolved inorganic carbon (DIC) isotopic signatures due to petrochemical CO_2

The addition of petrochemical CO_2 has drastically modified the isotopic signature of ambient DIC in the culture medium. The initial δ^{13}C-DIC of ~6 ‰ was progressively replaced by the much ^{13}C depleted carbon of petrochemical CO_2. These changes in δ^{13}C-DIC were rapid and took place during the exponential growth phase suggesting a combined action of algal assimilation, which removed ambient DIC and continuous supply of depleted petrochemical carbon. This rapid turnover of ambient DIC resulted from high biomass production along with the experiment. A simple (and probably oversimplified) POC mass balance model indicated that as soon as t_5, 93% of produced POC (9300 µmol.L^{-1} or µM) was supported by the added CO_2; the initial DIC level (~700 µmol.L^{-1} or µM) can only explain 7% of the POC production in case of full assimilation. Furthermore, at $t_{10,}$ the mass balance model indicated that 96% of assimilated DIC was of petrochemical origin. Accordingly, the predicted value of δ^{13}C-DIC using a binary mixing model was of -28.3‰ at t_5, which was substantially heavier (by 12.7‰) than the measured one -15.6‰. However, from t_{10} to t_{24}, predicted values of δ^{13}C-DIC were quite close to those measured. This deviation at t_5 observed during the exponential phase might be related to a non-conservative behavior of DIC.

4.3. Isotopic compositions of POC and isotopic fractionation during culture growth

The rapid and robust decrease observed in the bulk POC isotopic composition (δ^{13}C-POC) of *C. muelleri* was closely related to the highly depleted δ^{13}C-DIC injected in the ambient medium. The decrease in δ^{13}C-POC during the exponential growth phase (from t_0 to t_5) was especially fast in comparison with the decrease during

Phase II (t_{10} to t_{14}). The isotopic modification introduced in the inorganic substrate was rapidly transferred to the organic compartment during photosynthesis and underlined (if still necessary) the tight relationship existing between these two carbon pools. Marine algae are currently experiencing a similar isotopic modification due to the increase of anthropogenic CO_2 in the surface ocean. Anthropogenic CO_2, mostly derived from fossil fuels with light isotopic composition, tend to decrease the isotopic composition of natural DIC. This current modification is by far of much less amplitude than in our culture. Still, it represents a potential source of variation that is probably already registered in marine organic matter.

Isotopic fractionation in POC obtained in this study ranged between 11.7‰ (Phase I) and 19.0‰ (Phase II) when estimated using $\delta^{13}C\text{-}DIC_{TA}$ and between 15.3‰ and 24.9‰ when estimated with $\delta^{13}C\text{-}DIC_{M}$. Overall, these values fall within the range reported in the literature (Table 5). A fractionation value of 17‰ was obtained for *Phaeodactylum tricornutum* [22] and 18.5‰ for *Skeletonema costatum* [10]. Carbon isotopic composition can be influenced by the isotopic composition of the substrate, microalgae physiology, temperature, or enzyme responsible for carbon fixation [8, 45].

Table 5: Fractionation factor (ε_P), CO_2 concentrations and growth rates (μ) measured in other studies for diatoms

Taxon	Culture condition	ε_P (‰)	$[CO_{2aq}]$ ($\mu mol.kg^{-1}$)	μ (d^{-1})	References
Phaeodactylum tricornutum	Chemostat	25.72	34.7	0.5	Laws, et al. [12]
	Nitrate-limited	16.76	2.93	0.75	
	T=22°C	18.36	10.27	1.40	
Porosira glacialis	Chemostat	22.22	79.90	0.17	Popp, et al. [19]
	Continuous light	18.15	23.08	0.21	
	T°C (-0,1 or 2,0°C)	15.69	23.00	0.09	
Phaeodactylum tricornutum	Batch culture Continuous light Nutrient repleted T=15°C	10-16.7	0-40	1.6	Burkhardt, et al. [22]
Skeletonema costatum	Continuous light, Nutrient enriched T=15°C	12.4 14.1	2.6 25.5	1.7 1.9	Burkhardt, et al. [46]
Phaeodactylum tricornutum	Continuous light Nutrient enriched	16.7	37.7	1.6	Burkhardt, et al. [46]

	T=15°C Continuous light				
Thalassiosira weissflogii	Nutrient enriched	12.1	3.5	1.6	Burkhardt, et al. [46]
	T=15°C Continuous light	14.3	25.8	1.6	
Thalassiosira punctigera	Nutrient enriched T=15°C	12.1	30.1	0.9	Burkhardt, et al. [46]
Skeletonema costatum	12:12 cycle F/2 medium T°=18-22°C	18.6			Boller, et al. [10]

The temperature was not modified during the experiment and so should not be involved in fractionation factor variations. Due to the continuous CO_2 bubbling, in our experimental design, it was assumed that the algae were receiving a sufficient amount of CO_2 by passive diffusion. Thus, CO_2 levels were not a limiting factor to sustain its photosynthesis and development and unlikely required activation of carbon concentrating mechanisms (CCM) known to have a noteworthy kinetic effect on carbon isotopic composition. Concurrent conclusion with CO_2 concentration higher than 10 $\mu mol.kg^{-1}$ has already been made by Laws, et al. [12].

Flow cytometry monitoring of FSC and SSC, which are proxies of cell size and cell complexity, respectively [47-49], revealed an interesting relationship with carbon fractionation factor. FSC/SSC ratio and $\varepsilon_{P,TA}$ were negatively correlated. This meant that morphological changes of the cells may modify the way carbon is assimilated for growth and photosynthesis. Hypothetically, smaller cells with lower complexity (i.e cells undergoing such morphological changes) may not have an optimal exchange surface with CO_2 diffusion, thus inducing a stronger associated fractionation factor. A similar observation was made with chlorophyll content being negatively correlated to the fractionation factor. Overall, as the FSC/SSC ratio and chlorophyll content decreased with aging cells and decreasing cell division, these relationships may reflect that the fractionation factor increased with decreasing growth rate during our batch culture. This appeared in agreement with previous studies stating that the fractionation factor is expected to increase when the growth rate decreases [8, 45].

In addition to the influence of factors mentioned above, it has been shown that carbon fractionation can vary substantially according to RUBISCO types [10, 11, 50]. Five forms (IA, IB, IC, ID, and II) of RUBISCO have been identified in the past years [51]. Form I enzyme consists of eight large and eight small subunits, while form

II are dimers of single subunit homologous to form I large subunit [10]. Forms IA, IB, IC, and ID have been found in marine habitats in cyanobacteria and proteobacteria, eukaryotic green chloroplast or in diatoms, coccolithophores, rhodophytes and some dinoflagellates [10]. The fractionation factor associated with RUBISCO carboxylation, estimated for the diatom *Skeletonema costatum,* was equal to 18.5‰, this was assimilated to the form ID of RUBISCO [10]. However, Popp, et al. [19] and Laws, et al. [12] found higher fractionation factors with the diatom *Porosira glacialis* and *Phaeodactylum tricornutum* (22.2‰ and 25.7‰, respectively). Considering both variations of fractionation factors according to diatom species or culture phase within species, it is difficult to conclude how the respective RUBISCO types, experimental design, or physiology influenced carbon isotopic fractionation in the different studies. Carbon fractionation in diatom might then be more complex than the only isotopic effect associated with RUBISCO forms as previous studies revealed fairly large differences of fractionation factor within one species such as *Phaeodactylum tricornutum* [12, 19, 46]

4.4. Fatty acid composition of neutral and polar lipids

The fatty acid profiles found in *C. muelleri* were close to those identified in previous studies, the predominance of 16:0, 16:1n-7, 16:3n-4, and 20:5n-3 with the three latter being markers of diatoms [52-55]. The lipid analyses performed here covered the exponential phase (Phase I – t_5) and the stationary phase (Phase II – t_{10} and t_{14}) as FA production was limited during Phase III (microalgae senescence). The highest enrichment in NL by *C. muelleri* took place during Phase II as shown by BODIPY dynamics (Figure 2) and an increase in NL proportions and concentrations with time (Figure 7 and Table 3). Indeed when nutrients became scarce (as demonstrated by a slowdown in growth between Phases I and II), microalgae tended to accumulate lipids [56-58]. The CO_2 supply remaining stable throughout the experiment, the photosynthetic system was still able to maintain lipid production. These culture phase-dependent variations of lipid fraction concentrations were associated with the modification of fatty acids content. As shown in Table 3 and with PCA analysis (Figure 8), C16 fatty acids (16:0 and 16:1n-7) and 18:1n-9 in PL increased through time while others such as 20:5n-3, 16:3n-4 and 14:0 decreased. Similar observations can be made in the NL fraction, where 16:0 increased when 20:5n-3 or 14:0 decreased. On the contrary, other fatty acids (such as n-6 PUFA 18:3n-6 and 20:4n-6) remained relatively constant with time in both fractions. Fatty acids compositions changing with growth phases in *C. muelleri* may consequently affect their carbon isotopic signatures.

4.5. Isotopic composition of fatty acids in neutral and polar lipids

Because of the petrochemical carbon supply, the isotopic composition of total fatty acids of NL and PL fractions was highly depleted ranging from -52.9 ± 1.5‰ to -58.2 ± 1.1‰ and from -54.1 ± 2.6‰ to -57.2 ± 1.6‰, respectively as compared to natural phytoplankton fatty acids (-28 to -36‰) [59, 60]. Total FA isotopic signatures of both of NL and PL fractions were always more depleted in ^{13}C in comparison with bulk carbon (POC). Other studies previously observed such higher ^{13}C depletion into lipids [13, 28, 61, 62]. Except 18:4n-3 at t_5 and 18:1n-7 and 18:1n-9 at t_{10} and t_{14}, isotopic signatures of FA were similar between NL and PL during the whole experiment, suggesting they rapidly equilibrate between structural and reserve lipids in diatoms.

As fractionation varied according to culture phases, the fatty acids isotopic signatures are discussed for Phase I (exponential growth phase – t_5) and Phase II (stationary phase – t_{10} and t_{14}).

The high ^{13}C depletion and fractionation during Phase I revealed large differences of isotopic compositions between FA. Depending on the importance of the considered fatty acid during exponential growth phase, the FA synthesis efficiency and production may vary. PUFA such as 16:3n-4, 18:4n-3, and 20:5n-3 had more strongly depleted ^{13}C signatures than other fatty acids such as 14:0, 16:0, 16:1n-7, or 18:1n-9. Formation of the latter SFA and MUFA could then be assumed to be faster as their $\Delta_{FA\text{-}POC}$ were low, i.e. their isotopic compositions were close to those of POC. Thus, their productions were associated with less additional isotopic effects and consequently more facilitated, quicker than longer chain PUFA. Taipale, et al. [63] also reported that 16:3n-4 and 20:5n-3 presented a lower $\delta^{13}C$ than 16:1n-7 or 18:1n-9. Fractionation of 16:3n-4, 18:4n-3, and 20:5n-3 in comparison with POC was above 8‰ (Table 4). These PUFA are produced through complex enzymatic processes involving desaturases and elongase (for 20:5n-3) from their monounsaturated precursors (16:1n-7 for 16:3n-4 and 18:1n-9 for 18:4n-3 and 20:5n-3) [64-67]. However, it is unclear how the isotopic effect occurs during desaturation as carbons are not modified in this enzymatic process. Such isotopic effect(s) of desaturation during exponential growth is also supported by the lower depletion of averaged $\delta^{13}C$ of SFA and MUFA as compared to those of PUFA.

Within PUFA, differences of isotopic composition were observed between n-6 and n-3 PUFA. n-6 PUFA were always less depleted in ^{13}C than n-3 PUFA in both NL and PL fractions (the difference between weighted averages of 4‰ and 5‰ respectively). They seemed to have different roles and regulation during the exponential growth phase. Indeed, n-6 PUFA synthesis appeared faster (lower $\Delta_{FA\text{-}POC}$, less depleted in ^{13}C) than n-4 and n-3 PUFA synthesis (higher $\Delta_{FA\text{-}POC}$, more depleted in ^{13}C). Consequently, efficient synthesis *de novo* of n-4 and n-3

PUFA might be involved in different cellular and physiological roles than n-6 PUFA in *C. muelleri* fitness and growth during the exponential growth phase. 20:5n-3 and 16:3n-4 were identified as essential for diatoms development or stress resistance [68-72].

On the contrary to other PUFA, 18:4n-3 was less depleted in NL than in PL during exponential growth. Both membrane and reserve lipids shared parts of their biosynthesis pathway because they are both relying on the synthesis of diacylglycerol (DAG). DAG is formed from glycerol-3-phosphate (G3P) with a combination of two acyl chains at position *sn*-1 and *sn*-2 of the glycerol backbone. TAG is formed from DAG by an additional acylation at position *sn*-3. Consequently, this latest fixation of an acyl-chain at position *sn*-3, which is a significant difference between NL and PL pools, might be responsible for an additional isotopic effect discriminating their isotopic composition. At the opposite, fatty acids such as 16:1n-7, 16:3n-4, and 20:5n-3 for which isotopic signatures are very similar between lipids fractions might indicate a closer link.

Regarding the stationary phase (Phase II), there were fewer differences of isotopic signatures between fatty acids. They tended to reach value near -58.2‰ for NL and near -57.2‰ for PL. These observations were associated with lower $\Delta_{FA\text{-}POC}$ values in NL and PL. At the opposite of Phase I, SFA and MUFA ended up being more depleted than PUFA (-58.3‰ versus -56.4‰). During Phase II, 20:5n-3 presented one of the lowest $\Delta_{FA\text{-}POC}$. As mentioned earlier, a low $\Delta_{FA\text{-}POC}$ might correspond to a more active synthesis with less isotopic effects in comparison with the POC signature. We showed that 20:5n-3 proportions were decreasing in both NL and PL fractions during the stationary phase (Phase II). A more active synthesis might be initiated to limit the decrease of this important FA for *C. muelleri*. In parallel, increasing proportion FA such as 16:0 and 16:1n-7 presented isotopic composition with a higher difference in comparison with POC (difference of -4.1‰ to -5.3‰ versus -1.5‰ for 20:5n-3) associated to probable slower synthesis. During Phase II, 20:5n-3 isotopic composition was closer to those of 20:4n-6 than to those of 18:4n-3 which contrasted with Phase I. It is then possible that other synthesis pathways could be activated during Phase II to enhance the production of essential FA of interest (here 20:5n-3). The existence of two different pathways to synthesize 20:5n-3 in diatoms has already been suggested elsewhere [65, 67]. In diatoms, n-3 and n-6 PUFA pathways can be connected in microalgae by desaturation reaction by methyl-end desaturases gathered under the term ω-3 desaturases (Δ15, Δ17, Δ19). These reactions can form n-3 PUFA with n-6 PUFA as precursors [64, 65, 73]. In our study, it concerned the production of 18:4n-3 from 18:3n-6 and 20:5n-3 from 20:4n-6. In both cases, if this metabolic step did occur to form n-3 PUFA during Phase II, the methyl-end desaturation did not present significant fractionation.

Finally, the case of 18:1n-9 and 18:1n-7 was interesting at the end of Phase II: a large difference was observed between NL and PL isotopic composition for these fatty acids at t_{14}. While their isotopic compositions in the NL seemed close to those of other fatty acids, their isotopic composition in PL was close to POC signature ($\Delta_{FA\text{-}POC}$ = 0.1 ± 1.2‰ and $\Delta_{FA\text{-}POC}$ = 0.4 ± 2.0‰ respectively for 18:1n-9 and 18:1n-7). We hypothesized that bacteria might produce 18:1n-9 in PL at this point. Heterotrophic bacteria were previously described as presenting a very low fractionation in comparison with POC [63]. Such origin of 18:1n-9 is supported by the increase of bacteria concentration at the end of the culture (Figure 1B).

5. CONCLUSION

In the present study, fractionation of *Chaetoceros muelleri* POC was shown to vary according to culture phase and cell physiology, as revealed by the negative correlations between fractionation and both FSC/SSC ratio and chlorophyll content. FA isotopic signatures in both reserve (NL fraction) and structure lipids (PL fraction) were overall similar and always more depleted than POC. Proportions and isotopic of individual FA as compared to POC varied according to the culture phase. Some FA (14:0, 16:3n-4, 18:4n-3 and 20:5n-3) were in higher proportion and more depleted (as compared to POC) during the exponential phase than during the stationary phase while it was the opposite dynamic for 16:0.

Consequently, care must be undertaken while conducting ecological and biogeochemical studies using CSIA on fatty acids as it may provide different information depending on the physiological stages at which phytoplankton cells are collected. As the proportion of reserve lipids (NL) is known to increase when phytoplankton reach the stationary phase, this parameter might be useful to deconvolute and understand isotopic signature recorded in individual FA.

Finally, using petrochemical CO_2 allowed to produce algal biomass strongly depleted in ^{13}C (POC isotopic composition ranging from -48.7 to -57.0 ‰ according to culture age) can advantageously be used in ecological and trophic transfer studies as well as for studying biological-related processes such as synthesis pathways.

6. REFERENCES

1. Thompson, P.A., Guo, M.X., and Harrisson, P.J. (1992). Effects of variation in temperature. I. on the biochemical composition of eight species of marine phytoplankton. Journal of Phycology *28*, 481-488.
2. Thompson, P.A., Guo, M.X., Harrisson, P.J., and Whyte, J.N.C. (1992). Effects of variation in temperature. II. on the fatty acid composition of eight species of marine phytoplankton. Journal of Phycology *28*, 488-497.
3. Rousch, J.M., Bingham, S.E., and Sommerfeld, M. (2003). Changes in fatty acid profiles of thermo-intolerant and thermo-tolerant marine diatoms during temperature stress. Journal of Experimental Marine Biology and Ecology *295*, 145-156.
4. Rousseaux, C., and Gregg, W. (2014). Interannual Variation in Phytoplankton Primary Production at A Global Scale. Remote Sensing *6*, 1-19.
5. Gruber, N., and Keeling, C.D. (2001). An improved estimate of the isotopic air-sea disequilibrium of CO2: implications for the oceanic uptake of anthropogenic CO2. Geophysical Research Letters *28*, 555-558.
6. Ohkouchi, N., Ogawa, N.O., Chikaraishi, Y., Tanaka, H., and Wada, E. (2015). Biochemical and physiological bases for the use of carbon and nitrogen isotopes in environmental and ecological studies. Progress in Earth and Planetary Science *2*.
7. Fogel, M.L., and Cifuentes, L.A. (1993). Isotope fractionation during primary production. M.H.E.a.S.A. Macko, ed. (New York: Plenum Press), pp. 73-98.
8. Fry, B. (1996). 13C/12C fractionation by marine diatoms. Marine Ecology Progress Series *134*, 283-294.
9. Descolas-Gros, C., and Fontugne, M.R. (1990). Stable carbon isotope fractionation by marine phytoplankton during photosynthesis. Plant, Cell and Environment *13*, 207-218.
10. Boller, A.J., Thomas, P.J., Cavanaugh, C.M., and Scott, K.M. (2015). Isotopic discrimination and kinetic parameters of RubisCO from the marine bloom-forming diatom, Skeletonema costatum. Geobiology *13*, 33-43.
11. Roeske, C.A., and O'Leary, M.H. (1984). Carbon Isotope Effects on the Enzyme-Catalyzed Carboxylation of Ribulose Bisphosphatet. Biochemistry *23*, 6275-6284.
12. Laws, E.A., Bidigare, R.R., and Popp, B.N. (1997). Effect of growth rate and CO2 concentration on carbon isotopic fractionation by the marine diatom Phaeodactylum tricornutum. Limnology and Oceanography *42*, 1552-1560.
13. Fang, J., Abrajano, T.A., Comet, P.A., Brooks, J.M., Sassen, R., and MacDonald, I.R. (1993). Gulf of Mexico hydrocarbon seep communities xI. Carbon isotopic fractionation during fatty acid biosynthesis of seep organisms and its implication for chemosynthetic processes. Chemical Geology (Isotope Geoscience Section) *109*, 271-279.
14. Degens, E.T., Behrendt, M., Gotthardt, B., and Reppmann, E. (1968). Metabolic fractionation of carbon isotopes in marine plankton--II. Data on samples collected off the coasts of Peru and Ecuador. Deep Sea Research and Oceanographic Abstracts *15*, 11-20.
15. Degens, E.T., Guillard, R.R.L., Sackett, W.M., and Hellebust, J.A. (1968). Metabolic fractionation of carbon isotopes in marine plankton—I. Temperature and respiration experiments. Deep Sea Research and Oceanographic Abstracts *15*, 1-9.
16. Durako, M.J., and Sackett, W.M. (1992). Influence of carbon source on the stable carbon isotopic composition of the seagrass Thalassia testudinum. Marine Ecology Progress Series *86*, 99-101.
17. Hinga, K.R., Arthur, M.A., Pilson, M.E.Q., and Whitaker, D. (1994). Carbon isotope fractionation by marine phytoplankton in culture : the effects of CO2 concentration, pH, temperature and species. Global Biogeochemical Cycles *8*, 92-102.
18. Thompson, P.A., and Calvert, S.E. (1994). Carbon-isotope fractionation by a marine diatom: The influence of irradiance, daylength, pH, and nitrogen source. Limnology and Oceanography *39*, 1835-1844.
19. Popp, B.N., Laws, E.A., Bidigare, R.R., Dore, J.E., Hanson, K.L., and Wakeham, S.G. (1998). Effect of phytoplankton cell geometry on carbon isotopic fractionation. Geochimica et Cosmochimica Acta *62*, 69-77.
20. Rost, B., Riebesell, U., Burkhardt, S., and Sültemeyer, D. (2003). Carbon acquisition of bloom-forming marine phytoplankton. Limnology and Oceanography *48*, 55-67.
21. Benthien, A., Zondervan, I., Engel, A., Hefter, J., Terbrüggen, A., and Riebesell, U. (2007). Carbon isotopic fractionation during a mesocosm bloom experiment dominated by Emiliania huxleyi: Effects of CO2 concentration and primary production. Geochimica et Cosmochimica Acta *71*, 1528-1541.

22. Burkhardt, S., Riebesell, U., and Zondervan, I. (1999). Effects of growth rate, CO2 concentration, and cell size on the stable carbon isotope fractionation in marine phytoplankton. Geochimica et Cosmochimica Acta *63*, 3729-3741.
23. Laws, E.A., Popp, B.N., Bidigare, R.R., Kennicutt, M.C., and Macko, S.A. (1995). Dependence of phytoplankton carbon isotopic composition on growth rate and [CO2aq]: Theoretical considerations and experimental results. Geochimica et Cosmochimica Acta *59*, 1131-1138.
24. Sharkey, T.D., and Berry, J.A. (1985). Carbon isotope fractionnation of algae as influenced by and inducible CO2 concentration mecanism. In Inorganic carbon uptake by aquatic photosynthetic organisms, WJ Lucas and Berry Edition Edition., pp. 389-401.
25. Abelson, P.H., and Hoering, T.C. (1961). Carbon isotope fractionation in formation of amino acids by photosynthetic organisms. Proceeding of the National Academy of Sciences *47*, 623-632.
26. Park, R., and Epstein, S. (1961). Metabolic fractionation of 13C and 12C in plants. Plant Physiology *36*, 133-138.
27. DeNiro, M., and Epstein, S. (1977). Mechanism of carbon isotope fractionation associated with lipid synthesis. Science *197*, 261-263.
28. Monson, D.K., and Hayes, J.M. (1982). Carbon isotopic fractionation in the biosynthesis of bacterial fatty acids. Ozonolysis of unsaturated fatty acids as a means of determining the intramolecular distribution of carbon isotopes. Geochimica et Cosmochimica Acta *46*, 139-149.
29. Hayes, J.M. (2001). Fractionation of Carbon and Hydrogen Isotopes in Biosynthetic Processes. Reviews in Mineralogy and Geochemistry *43*, 225-277.
30. Schouten, S., Klein Breteler, W.C.M., Blokker, P., Schogt, N., Rijpstra, W.I.C., Grice, K., Baas, M., and Sinninghe Damsté, J.S. (1998). Biosynthetic effects on the stable carbon isotopic compositions of algal lipids: implications for deciphering the carbon isotopic biomarker record. Geochimica et Cosmochimica Acta *62*, 1397-1406.
31. Lelong, A., Haberkorn, H., Le Goïc, N., Hégaret, H., and Soudant, P. (2011). A New Insight into Allelopathic Effects of Alexandrium minutum on Photosynthesis and Respiration of the Diatom Chaetoceros neogracile Revealed by Photosynthetic-performance Analysis and Flow Cytometry. Microbial Ecology *62*, 919-930.
32. Seoane, M., González-Fernández, C., Soudant, P., Huvet, A., Esperanza, M., Cid, A., and Paul-Pont, I. (2019). Polystyrene microbeads modulate the energy metabolism of the marine diatom Chaetoceros neogracile. Environmental Pollution *251*, 362-371.
33. Assayag, N., Rivé, K., Ader, M., Jézéquel, D., and Agrinier, P. (2006). Improved method for isotopic and quantitative analysis of dissolved inorganic carbon in natural water samples. Rapid Communications in Mass Spectrometry *20*, 2243-2251.
34. Schimmelmann, A., Albertino, A., Sauer, P.E., Qi, H., Molinie, R., and Mesnard, F. (2009). Nicotine, acetanilide and urea multi-level 2H-, 13C- and 15N-abundance reference materials for continuous-flow isotope ratio mass spectrometry. Rapid Communications in Mass Spectrometry *23*, 3513-3521.
35. Lewis, E., and Wallace, D. (1998). CO2SYS Program developed for CO2 system calculations. In ORNL/CDIAC-105. (Oak Ridge, Tennessee: Department of Applied Science, Brookhaven National Laboratory), p. 42.
36. Rau, G.H., Riebesell, U., and Wolf-Gladrow, D.A. (1996). A model of photosynthetic 13C fractionation by marine phytoplankton based on diffusive molecular CO2 uptake. Marine Ecology Progress Series *133*, 275-285.
37. Freeman, K.H., and Hayes, J.M. (1992). Fractionation of carbon isotopes by phytoplankton and estimates of ancient CO2 levels. Global Biogeochemical Cycles *6*, 185-198.
38. Salvesen, I., Reitan, K.I., Skjermo, J., and Øie, G. (2000). Microbial environments in marine larviculture: Impacts of algal growth rates on the bacterial load in six microalgae. Aquaculture International *8*, 275-287.
39. Le Grand, F., Soudant, P., Siah, A., Tremblay, P., Marty, Y., and Kraffe, E. (2014). Disseminated Neoplasia in the Soft-Shell Clam Mya arenaria: Membrane Lipid Composition and Functional Parameters of Circulating Cells. Lipids *49*, 807-818.
40. Mathieu-Resuge, M., Schaal, G., Kraffe, E., Corvaisier, R., Lebeau, O., Lluch-Costa, S.E., Salgado García, R.L., Kainz, M.J., and Le Grand, F. (2019). Different particle sources in a bivalve species of a coastal lagoon: evidence from stable isotopes, fatty acids, and compound-specific stable isotopes. Marine Biology *166*, 89-101.
41. R Core Team (2019). A language and environment for statistical computing. Volume 2020, R.F.f.S. Computing, ed. (Vienna, Austria).
42. Geider, R., Platt, T., and Raven, J.A. (1986). Size dependence of growth and photosynthesis in diatoms: a synthesis. Marine Ecology Progress Series *30*, 93-104.

43. George, B., Pancha, I., Desai, C., Choksi, K., Paliwal, C., Ghosh, T., and Mishra, S. (2014). Effects of different media composition, light intensity and photoperiod on morphology and physiology of freshwater microalgae Ankistrodesmus falcatus – A potential strain for bio-fuel production. Bioresource Technology *171*, 367-374.
44. Li, Y., Horsman, M., Wang, B., Wu, N., and Lan, C.Q. (2008). Effects of nitrogen sources on cell growth and lipid accumulation of green alga Neochloris oleoabundans. Applied Microbiology and Biotechnology *81*, 629-636.
45. Michener, R.H., and Kaufman, L. (2007). Stable isotope as tracers in marine food webs: an update. In Stable isotopes in ecology and environmental science, 2nd edition Edition, R. Michener and K. Lajtha, eds. (Malden, USA, Oxford, UK, Carlton, Australia: Blackwell), pp. 22-60.
46. Burkhardt, S., Riebesell, U., and Zondervan, I. (1999). Stable carbon isotope fractionation by marine phytoplankton in response to daylength, growth rate, and CO2 availability. Marine Ecology Progress Series *184*, 31-41.
47. Tracy, B.P., Gaida, S.M., and Papoutsakis, E.T. (2010). Flow cytometry for bacteria: enabling metabolic engineering, synthetic biology and the elucidation of complex phenotypes. Current Opinion in Biotechnology *21*, 85-99.
48. Le Goïc, N., Hegaret, H., Boulais, M., Béguel, J.-P., Lambert, C., Fabioux, C., and Soudant, P. (2014). Flow cytometric assessment of morphology, viability, and production of Reactive Oxygen Species of Crassostrea gigas oocytes. Application to toxic Dinoflagellate (Alexandrium minutum) exposure. Cytometry Part A *85A*, 1049-1056.
49. González-Fernández, C., Toullec, J., Lambert, C., Le Goïc, N., Seoane, M., Moriceau, B., Huvet, A., Berchel, M., Vincent, D., Courcot, L., et al. (2019). Do transparent exopolymeric particles (TEP) affect the toxicity of nanoplastics on Chaetoceros neogracile? Environmental Pollution *250*, 873-882.
50. Robinson, J.J., Scott, K.M., O'Leary, M.H., Horken, K., Tabita, F.R., and Cavanaugh, C.M. (2003). Kinetic isotope effect and characterization of form II RubisCO from the chemoautotrophic endosymbionts of the hydrothermal vent tubeworm Riftia pachyptila. Limnology and Oceanography *48*, 48-54.
51. Tabita, F.R., Hanson, T.E., Li, H., Satagopan, S., Singh, J., and Chan, S. (2007). Function, Structure, and Evolution of the RubisCO-Like Proteins and Their RubisCO Homologs. Microbiology and Molecular Biology Reviews *71*, 576-599.
52. Volkman, J.K., Jeffrey, S.W., Nichols, P.D., Rogers, G.I., and Garland, C.D. (1989). Fatty acid and lipid composition of 10 species of microalgae used in mariculture. Journal of Experimental Marine Biology and Ecology *128*, 219-240.
53. Hatate, H., Ohgai, M., Murase, N., Miyake, N., and Suzuki, N. (1998). Accumulation of fatty acids in Chaetoceros gracilis (Bacillariophyceae) during stationary growth phase. Fisheries Science *64*, 578-581.
54. Vazhappilly, R., and Chen, F. (1998). Eicosapentaenoic acid and docosahexaenoic acid production potential of microalgae and their heterotrophic growth. Journal of the American Oil Chemists' Society *75*, 393-397.
55. Pernet, F., Tremblay, R., Demers, E., and Roussy, M. (2003). Variation of lipid class and fatty acid composition of Chaetoceros muelleri and Isochrysis sp. grown in a semicontinuous system. Aquaculture *221*, 393-406.
56. Courchesne, N.M.D., Parisien, A., Wang, B., and Lan, C.Q. (2009). Enhancement of lipid production using biochemical, genetic and transcription factor engineering approaches. Journal of Biotechnology *141*, 31-41.
57. Li, X., Hu, H.Y., Gan, K., and Sun, Y.X. (2010). Effects of different nitrogen and phosphorus concentrations on the growth, nutrient uptake, and lipid accumulation of a freshwater microalga Scenedesmus sp. Bioresource Technology *101*, 5494-5500.
58. Xu, D., Gao, Z., Li, F., Fan, X., Zhang, X., Ye, N., Mou, S., Liang, C., and Li, D. (2013). Detection and quantitation of lipid in the microalga Tetraselmis subcordiformis (Wille) Butcher with BODIPY 505/515 staining. Bioresource Technology *127*, 386-390.
59. Budge, S.M., Wooller, M.J., Springer, A.M., Iverson, S.J., McRoy, C.P., and Divoky, G.J. (2008). Tracing carbon flow in an arctic marine food web using fatty acid-stable isotope analysis. Oecologia *157*, 117-129.
60. Kravchuk, E.S., Sushchik, N.N., Makhutova, O.N., Trusova, M.Y., Kalachova, G.S., and Gladyshev, M.I. (2014). Differences in carbon isotope signatures of polyunsaturated fatty acids of two microalgal species. Doklady Biochemistry and Biophysics *459*, 183-185.
61. Parker, P.L. (1961). The isotopic composition of the carbon of fatty acids. In Carnegie Institution of Washington Year Book, Volume 61, G. Press, ed. (Baltimore, Maryland: Carnegie Institution of Washington), pp. 187-190.

62. Parker, P.L. (1964). The biogeochemistry of the stable isotopes of carbon in a marine bay. Geochimica et Cosmochimica Acta *28*.
63. Taipale, S.J., Peltomaa, E., Hiltunen, M., Jones, R.I., and Hahn, M.W. (2015). Inferring Phytoplankton, Terrestrial Plant and Bacteria Bulk $\delta^{13}C$ Values from Compound Specific Analyses of Lipids and Fatty Acids. PLoS One *10*, e0133974.
64. Zulu, N.N., Zienkiewicz, K., Vollheyde, K., and Feussner, I. (2018). Current trends to comprehend lipid metabolism in diatoms. Progress in Lipid Research *70*, 1-16.
65. Remize, M., Planchon, F., Loh, A.N., Le Grand, F., Bideau, A., Le Goic, N., Fleury, E., Miner, P., Corvaisier, R., Volety, A., et al. (2020). Study of Synthesis Pathways of the Essential Polyunsaturated Fatty Acid 20:5n-3 in the Diatom Chaetoceros muelleri Using 13C-Isotope Labeling. Biomolecules *10*, 797.
66. Domergue, F., Spiekermann, P., Lerchl, J., Beckmann, C., Kilian, O., Kroth, P.G., Boland, W., Zahringer, U., and Heinz, E. (2003). New Insight into Phaeodactylum tricornutum Fatty Acid Metabolism. Cloning and Functional Characterization of Plastidial and Microsomal Delta 12-Fatty Acid Desaturases. Plant Physiology *131*, 1648-1660.
67. Arao, T., and Yamada, M. (1994). Biosynthesis of polyunsaturated fatty acids in the marine diatom, Phaeodactylum tricornutum. Phytochemistry *35*, 1177-1181.
68. d'Ippolito, G., Cutignano, A., Briante, R., Febbraio, F., Cimino, G., and Fontana, A. (2005). New C16 fatty-acid-based oxylipin pathway in the marine diatom Thalassiosira rotula. Organic & Biomolecular Chemistry *3*, 4065.
69. d'Ippolito, G., Tucci, S., Cutignano, A., Romano, G., Cimino, G., Miralto, A., and Fontana, A. (2004). The role of complex lipids in the synthesis of bioactive aldehydes of the marine diatom Skeletonema costatum. Biochimica et Biophysica Acta (BBA) - Molecular and Cell Biology of Lipids *1686*, 100-107.
70. Cutignano, A., d'Ippolito, G., Romano, G., Lamari, N., Cimino, G., Febbraio, F., Nucci, R., and Fontana, A. (2006). Chloroplastic Glycolipids Fuel Aldehyde Biosynthesis in the Marine Diatom Thalassiosira rotula. ChemBioChem *7*, 450-456.
71. Desbois, A.P., Lebl, T., Yan, L., and Smith, V.J. (2008). Isolation and structural characterisation of two antibacterial free fatty acids from the marine diatom, Phaeodactylum tricornutum. Applied Microbiology and Biotechnology *81*, 755-764.
72. Parrish, C.C. (2013). Lipids in Marine Ecosystems. ISRN Oceanography *2013*, 1-16.
73. Monroig, O., and Kabeya, N. (2018). Desaturases and elongases involved in polyunsaturated fatty acid biosynthesis in aquatic invertebrates: a comprehensive review. Fisheries Science *911-928*.